Universiteit Leiden
The Netherlands

Harnessing the immunostimulatory properties of oncolytic reovirus for anticancer immunotherapy

Groeneveldt, P.C.

Citation

Groeneveldt, P. C. (2023, November 23). *Harnessing the immunostimulatory properties of oncolytic reovirus for anticancer immunotherapy*. Retrieved from https://hdl.handle.net/1887/3663612

Version:	Publisher's Version
License:	Licence agreement concerning inclusion of doctoral thesis in the Institutional Repository of the University of Leiden
Downloaded from:	https://hdl.handle.net/1887/3663612

Note: To cite this publication please use the final published version (if applicable).

PART A

Exploitation of the reovirus-specific T-cell response for anticancer therapy

CHAPTER 2

Preconditioning of the tumor microenvironment with oncolytic reovirus converts CD3-bispecific antibody treatment into effective immunotherapy

Christianne Groeneveldt[1], Priscilla Kinderman[1], Diana J. M. van den Wollenberg[2], Ruben L. van den Oever[1], Jim Middelburg[1], Dana A. M. Mustafa[3], Rob C. Hoeben[2], Sjoerd H. van der Burg[1], Thorbald van Hall[1#] and Nadine van Montfoort[1#]

1 Department of Medical Oncology, Oncode Institute, Leiden University Medical Center, 2333 ZA, Leiden, The Netherlands

2 Department of Cell and Chemical Biology, Leiden University Medical Center, 2300 RC, Leiden, The Netherlands

3 Department of Pathology, the Tumor Immuno-Pathology Laboratory, Erasmus MC, University Medical Center Rotterdam, Rotterdam, 3000 CA, The Netherlands

Corresponding authors

Journal for ImmunoTherapy of Cancer 2020;8:e001191. doi:10.1136/jitc-2020-001191

ABSTRACT

Background. T-cell-engaging CD3-bispecific antibodies (CD3-bsAbs) are promising modalities for cancer immunotherapy. Although this therapy has reached clinical practice for hematological malignancies, the absence of sufficient infiltrating T cells is a major barrier to efficacy in solid tumors. In this study, we exploited oncolytic reovirus as a strategy to enhance the efficacy of CD3-bsAbs in immune-silent solid tumors.

Methods. The mutant *p53* and *K-ras*-induced murine pancreatic cancer model KPC3 resembles human pancreatic ductal adenocarcinomas with a desmoplastic tumor microenvironment, low T-cell density, and resistance to immunotherapy. Immune-competent KPC3-tumor bearing mice were intratumorally injected with reovirus type 3 Dearing strain and the reovirus-induced changes in the tumor microenvironment and spleen were analyzed over time by NanoString analysis, RT-qPCR, and multicolor flow cytometry. The efficacy of reovirus in combination with systemically injected CD3-bsAbs was evaluated in immune-competent mice with established KPC3 or B16.F10 tumors, and in the close-to-patient $HER2^+$ breast cancer model BT474 engrafted in NSG mice with human PBMCs as effector cells.

Results. Replication-competent reovirus induced an early IFN signature, followed by a strong influx of NK cells and $CD8^+$ T cells, at the cost of $FoxP3^+$ Tregs. Viral replication declined after seven days and was associated with systemic activation of lymphocytes and the emergence of intratumoral reovirus-specific $CD8^+$ T cells. Although tumor-infiltrating T cells were mostly reovirus-specific and not tumor-specific, they served as non-exhausted effector cells for the subsequently systemically administered CD3-bsAbs. Combination treatment of reovirus and CD3-bsAbs led to the regression of large, established KPC3, B16F10, and BT474 tumors. Reovirus as a preconditioning regimen performed significantly better than simultaneous or early administration of CD3-bsAbs. This combination treatment induced regressions of distant lesions that were not injected with reovirus, and systemic administration of both reovirus and CD3-bsAbs also led to tumor control. This suggests that this therapy might also be effective for metastatic disease.

Conclusions. Oncolytic reovirus administration represents an effective strategy to induce a local IFN response and strong T-cell influx, thereby sensitizing the tumor microenvironment for subsequent CD3-bsAb therapy. This combination therapy warrants further investigation in patients with non-inflamed solid tumors.

GRAPHICAL ABSTRACT

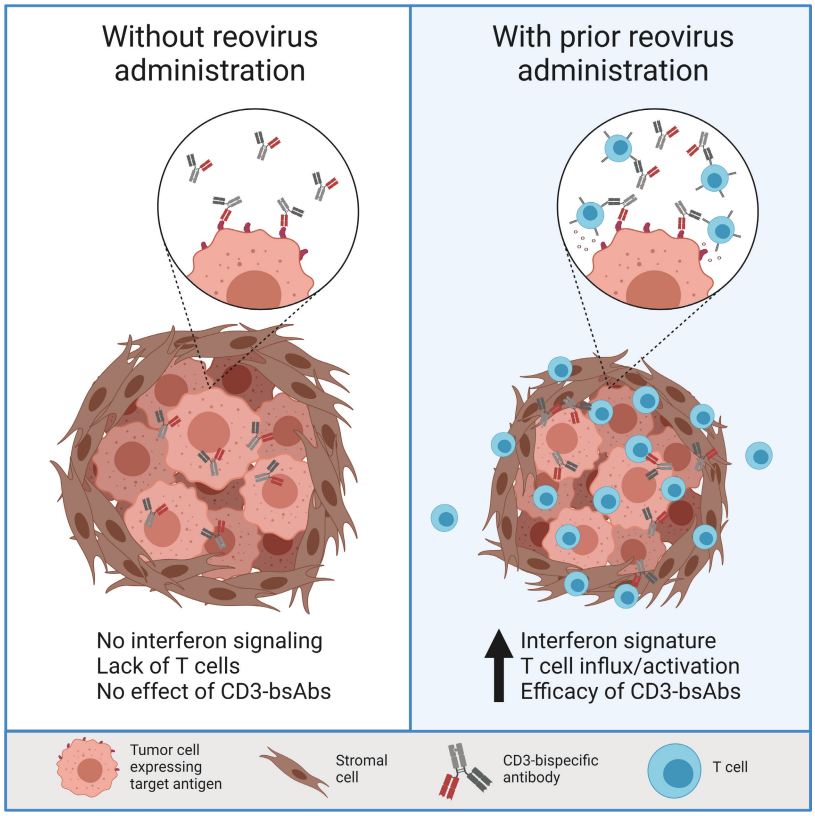

INTRODUCTION

T-cell-engaging bispecific antibodies (bsAbs) are emerging as a potent therapeutic cancer modality (1). These immunoglobulin-based biologicals can induce dramatic responses in advanced malignancies, as was demonstrated with the use of a CD3xCD19 bsAb for the treatment of non-Hodgkin's lymphoma (2). Currently, more than 40 other T-cell-redirecting bsAbs are in clinical development for both hematological malignancies and solid tumors (3). CD3-bsAbs are comprised of one arm engaging a tumor-associated antigen (TAA) expressed on the cell surface of cancer cells, and a second arm targeting T cells via CD3 (4). By tethering T cells to tumor cells, these CD3-bsAbs create a functional immunological synapse (5). This results in selective T-cell-mediated killing of the target-expressing tumor cells, for which both $CD4^+$ and $CD8^+$ T cells can be employed (6). Since binding and activation of T cells occurs via CD3, these CD3-bsAbs can activate T cells in an MHC class I- and T-cell receptor (TCR)-independent manner. CD3-bsAbs can redirect a large proportion of the polyclonal T-cell pool towards the tumor, and thereby bypass the need for endogenous tumor-specific T cells (7). Despite the many advantages of these CD3-bsAbs, clinical development has been hampered by several factors, including low response rates in solid, immune-silent tumors (7). Factors associated with poor response to immunotherapy include the absence of an interferon gene signature and lack of T cells in the tumor beds, generally referred to as a 'cold' microenvironment (8,9).

Oncolytic viruses (OVs) are increasingly recognized as potent anticancer moieties due to their virtue of selective replication in transformed cells and the ability to ignite an antiviral immune response in the malignant lesion (10). It has been demonstrated that OVs can sensitize resistant tumors for checkpoint blockade therapy (11-13). The mammalian reovirus type 3 Dearing strain (T3D), which is not associated with symptomatic disease in humans, is one of the leading oncolytic viruses under clinical evaluation and displays an excellent safety record in clinical trials (14,15). Reoviruses show an inherent preference for replication in transformed, but not in healthy cells (16,17). Although reovirus has demonstrated some tumor regressions as a monotherapy in certain cancer types, such as in prostate xenograft models and prostate cancer patients, its potency might be better manifested in rationally-designed combination strategies (18,19). In this study, we employed oncolytic reovirus as a strategy to enhance the antitumor efficacy of CD3-bsAbs in solid tumors. Using fully immunocompetent mouse tumor models, we demonstrated that injection with replication-competent reovirus converted immunologically cold pancreatic adenocarcinoma tumors to inflamed sites with a strong IFN signature and abundance of virus-specific $CD8^+$ T cells. This effect depended on viral replication, which was controlled by the immune system within two weeks. Subsequent systemic administration of bsAb resulted in regressions of local and distant large tumors. These findings provide evidence that preconditioning the tumor microenvironment with oncolytic reovirus is an attractive strategy to prime immune-silent tumors for effective CD3-bsAb therapy.

MATERIAL & METHODS

Reovirus

The wild-type reovirus strain R124 (here referred to as reovirus) was previously isolated from a heterogeneous reovirus Type 3 Dearing (T3D) stock (VR-824) obtained from the American Type Culture Collection (ATCC) by two rounds of plaque purification using HER911 cells (20). All experiments were performed using cesium chloride (CsCl)-purified stocks (see Supplementary materials). The total amount of particles was calculated based on OD260 values where 1 OD equals 2.10×10^{12} reovirus particles/mL (21). The infectious titer was quantified by plaque assay on HER911 cells (22). Reovirus particles were inactivated by exposure to shortwave ultraviolet light (254 nm) for 15 minutes at room temperature on a low-attachment 6-well plate (Corning™) (23). Afterward, the total amount of viral particles was determined based on the OD_{260} values. A correction value was calculated to ensure an equal number of viral particles for treatments with infectious and inactivated reovirus (UVi).

Bispecific antibodies

The CD3xTRP1 bispecific antibody (bsAb) used is a knob-into-hole bispecific based on murine IgG2a with an Fc Silent™ mutation, featuring one arm with an anti-mouse CD3e scFv based on the clone 145-2C11, and the other arm containing the TA99 clone directed against TRP1 (bAb0136; Absolute Antibody). The CD3xHER2 bsAb comprises an anti-human CD3 scFv based on the clone OKT3, together with an anti-HER2 arm based on clone 4D5-8 (Trastuzumab) (bAb0183; Absolute Antibody).

Cell lines

The murine pancreatic cancer cell line KPC3 is a low-passage derivate of a primary KPC tumor with mutant *p53* and *K-ras* (24) from a female C57BL/6 mouse. KPC3.TRP1 cells were generated as described (25) and selected for expression of TRP1 by cell sorting using an αTRP1 antibody (clone: TA99). The murine melanoma cell line B16.F10 (ATCC-CRL6475) and the human breast cancer cell line BT474 (ATCC-HTB-20) were purchased from the American Type Culture Collection. More information can be found in the **Supplementary Methods**.

Animal experiments

Male or female C57BL/6J mice (Charles River Laboratories, France) of 8 weeks old were used for the KPC3 and B16.F10 models, respectively. KPC3 or KPC3.TRP1 tumors were inoculated by subcutaneous injection of 1×10^5 (for antitumor efficacy experiments) or 2×10^5 (for intratumoral analysis experiments) cells in the right flank in 100-200 µL PBS/0.1% BSA. For bilateral experiments, a second tumor was subcutaneously engrafted one week after the primary tumor on the alternate flank. B16.F10 tumors were engrafted by subcutaneous injection of 5×10^4 cells in a volume of 100 µL PBS/0.1% BSA. Female NOD.Cg-Prkdc^{scid}Il2rg^{tm1Wjl}SzJ/ (NSG) mice of 6 weeks old (Charles River Laboratories, France) were used for the BT474 model. BT474 tumors were orthotopically

engrafted by injecting $5x10^6$ cells in a volume of 100 µL 50:50 PBS/0.1% BSA : Growth Factor Reduced matrigel (Corning®) in the fourth mammary fat pad of isoflurane-anesthetized mice. Human PBMCs from a buffy-coat of an anonymous consented donor (Sanquin Blood bank, Amsterdam, The Netherlands), HLA-A29:02-matched to BT474 (26), were isolated by Ficoll-Paque density-gradient centrifugation. $5x10^6$ PBMCs were intravenously administered to each mouse in a volume of 100 µL PBS/0.1% BSA.

Mice with palpable tumors were allocated into groups with similar average tumor volumes and assigned a treatment regimen. Intratumoral reovirus administration was performed by injection of 10^7 plaque-forming units (pfu) of reovirus or PBS as a control in a volume of 30 µL on 3 consecutive days unless otherwise indicated, while mice were under isoflurane anesthesia. Intravenous reovirus administration was performed by injection of 10^7 or 10^8 pfu of reovirus in a volume of 100 µL in the tail vein on 3 consecutive days. Treatment with CD3xTRP1 or CD3xHER2 bsAbs consisted of 3 intraperitoneal injections of 12,5 µg antibody in 100 µL PBS given every other day. Treatment with FTY720 (Cayman Chemical) occurred by supplementing the mice with 2,5 µg/mL FTY720 in their drinking water and a daily oral dose of 2 µg FTY720/g body weight administered orally via pipetting into the mouth. During all experiments, tumors were measured 3-6 times a week in 3 dimensions using a caliper, in a blinded manner concerning the experimental group. For antitumor efficacy experiments, mice were euthanized when tumors reached the experimental endpoint, which equals a volume of 1000 mm^3 (one-tumor model) or a combined volume of 1500 mm^3 (bilateral tumor model). Mice were censored from analysis when they had to be euthanized due to humane endpoints before reaching the experimental endpoint. For intratumoral analysis experiments, mice were sacrificed at indicated days after treatment before tumors and/or spleens were collected. Tumors were divided into representative parts, which were either snap-frozen in liquid N_2 and stored at -80 °C until further analysis, fixed in 4% formaldehyde (AddedPharma) for immunohistochemistry or immediately processed to single cells suspensions to analyze the cellular composition by flow cytometry. These procedures are described in detail in the **Supplementary Methods**.

Quantification of reovirus replication by RT-qPCR

Reovirus replication was quantified by quantitative reverse transcription polymerase chain reaction (RT-qPCR) of reovirus genomic segment 4 (S4) on RNA of cells, tumors, and other organs, as described in the **Supplementary Methods**. Reovirus S4 copy numbers were determined based on a standard curve, generated with serial dilutions of plasmid pcDNA_S4. Log_{10} S4 copy numbers were calculated using a previously described formula (27).

NanoString analysis

Total RNA was isolated from a representative piece (10-30 mg) of each tumor as described in the **Supplementary Methods**. RNA quality and integrity (RQI) were determined using the Experion™ Automated Electrophoresis System (Bio-Rad).

Only samples with an RQI score > 8 were included for NanoString analysis. Multiplex gene expression was measured using the PanCancer Mouse Immune Profiling panel (NanoString Technologies). 200 ng of total RNA was hybridized for 17 hours and quantified by scanning 490 Field of Views (FOV) using the Digital Analyzer (nCounter Flex). Data were processed and normalized using nSolver Analysis Software (version 4.0) and the Advanced Analysis module (NanoString). NanoString-defined markers were used to analyze cell type scores. Expression of reovirus-induced host genes was confirmed by RT-qPCR as described in the **Supplementary Methods**.

Statistics

All graphs were prepared and statistical analyses were performed using the GraphPad Prism software (version 8). All data represent mean±SEM and key data are representative of 2-5 experiments with similar results. Survival between groups was compared using Kaplan-Meier curves and the statistical log-rank test (Mantel-Cox). For RT-qPCR analysis, samples were excluded when RNA concentration and purity were too low. When comparing S4 RT-qPCR data between two groups, average Log_{10} values were compared using a two-tailed unpaired t test. For comparing more groups versus PBS treatment, average Log_{10} values were compared using an ordinary one-way analysis of variance (ANOVA) including Dunnett's post-hoc test. For flow cytometry data, tumor samples were excluded when evidence for draining lymph node contamination was present. The means of flow cytometric data of two experimental groups were compared using two-tailed unpaired t tests. For comparing multiple groups versus PBS treatment or negative control, a one-way analysis of variance (ANOVA) including Dunnett's post-hoc test was performed. For comparing multiple groups with each other, a one-way analysis of variance (ANOVA) including Tukey's post-hoc test was used. The association between two ranked variables was done by Spearman rank correlation. Significance levels are labeled with asterisks, with *p<0.05, **<0.01, ***p<0.001, and ****p<0.0001. Non-significant differences are indicated by ns.

RESULTS

Reovirus efficiently replicates but does not affect tumor growth in the KPC3 pancreatic cancer model

Human pancreatic tumors are often not susceptible to immunotherapeutic strategies, including checkpoint inhibition (28,29). The murine pancreatic cancer model KPC3 is an early derivate from the genetic pancreatic ductal adenocarcinoma (PDAC) KPC mouse model, which recapitulates many of the histopathological and immunological key features observed in human PDAC (30), including acinar tubular structures, a dense desmoplastic stroma, and absence of $CD3^+$ T cells (**Figure S1A, B**). We previously demonstrated that the outgrowth of KPC3 tumors with heterologous expression of the *Trp1* gene (KPC3.TRP1) could significantly be delayed by early CD3xTRP1 bsAb therapy (25). However, CD3xTRP1 bsAb treatment failed to exhibit any effect on larger KPC3.

TRP1 tumors (**Figure S1C, D**), although tumor cells were efficiently killed *in vitro* in an antigen-dependent fashion (**Figure S1E**). We hypothesized that the low T-cell density observed in established KPC3 tumors represents a major barrier to the efficacy of CD3-bsAb therapy and therefore explored the use of oncolytic reovirus to overcome this barrier.

We first tested the ability of reovirus to infect and replicate in KPC3 cells *in vitro* and observed a high number of genomic viral copies (**Figure 1A**) and reoviral protein $\sigma3^+$ cells (**Figure 1B**) after infection with very low multiplicities of infection (MOIs). Total viral copy numbers and viral load per cell increased with higher MOIs, and additionally, reovirus demonstrated a dose-dependent oncolytic activity *in vitro* (**Figure 1C**). Oncolytic activity appeared moderate as half of the cell culture was killed after 2 days, whereas all cells contained high levels of replicating virus. As expected, reovirus did not replicate after UV-inactivation (UVi) in KPC3 cell cultures (**Figure 1A**) (23). To test the replication capacity of reovirus *in vivo*, KPC3 tumor-bearing mice were intratumorally injected on three consecutive days with either 10^7 or 10^8 plaque-forming units (pfu)/mouse starting at day 13 when the tumors were established (**Figure 1D**). Both viral doses resulted in high levels of genomic reovirus copies after three days, indicating efficient replication *in vivo* (**Figure 1E**)**.** Hotspots of viral replication were seen in tumor tissue slides stained for σ3, suggesting that viral replication is not evenly distributed in the tumor (**Figure 1F**). Despite this very efficient replication, reovirus administration failed to make a large impact on tumor growth (**Figure 1G**). Since optimal replication was observed with 10^7 pfu/mouse, we selected this dose for further experiments.

Replication-competent reovirus induces a potent interferon response in the tumor

Next, we studied the kinetics of reovirus replication in KPC3 tumor-bearing mice (**Figure 2A**). Intratumoral administration of reovirus yielded high viral copy numbers that peaked around 1 to 3 days and gradually decreased back to baseline levels around day 11 post-injection (**Figure 2B**). UVi reovirus did not show any amplification. Thus, reovirus has a limited time window of replication in the tumor microenvironment which lasted up to 10 days, suggesting that replication is restricted by antiviral immunity of the host. Transcriptome analysis of whole KPC3 tumors using NanoString technology was performed to investigate the antiviral immune response (**Figure 2C and Figure S2A**). A heatmap of all genes differentially expressed on at least one of the time points revealed that the number of upregulated genes peaked 7 days after reovirus administration (**Figure 2C**). More than 100 immune-related genes were upregulated (FDR $p < 0.1$ and fold change > 2 compared to PBS) and this number severely declined after 11 days, in parallel with viral replication (**Figure 2C and Figure S2A**). Although UVi reovirus might still have the capacity to engage pattern-recognition receptors, as was previously demonstrated (31), this inactivated reovirus did not induce upregulation of immune genes (**Figure 2C and Figure S2A**). This suggested that the ability to replicate was essential for the immunostimulatory effects of reovirus in the tumor microenvironment (TME).

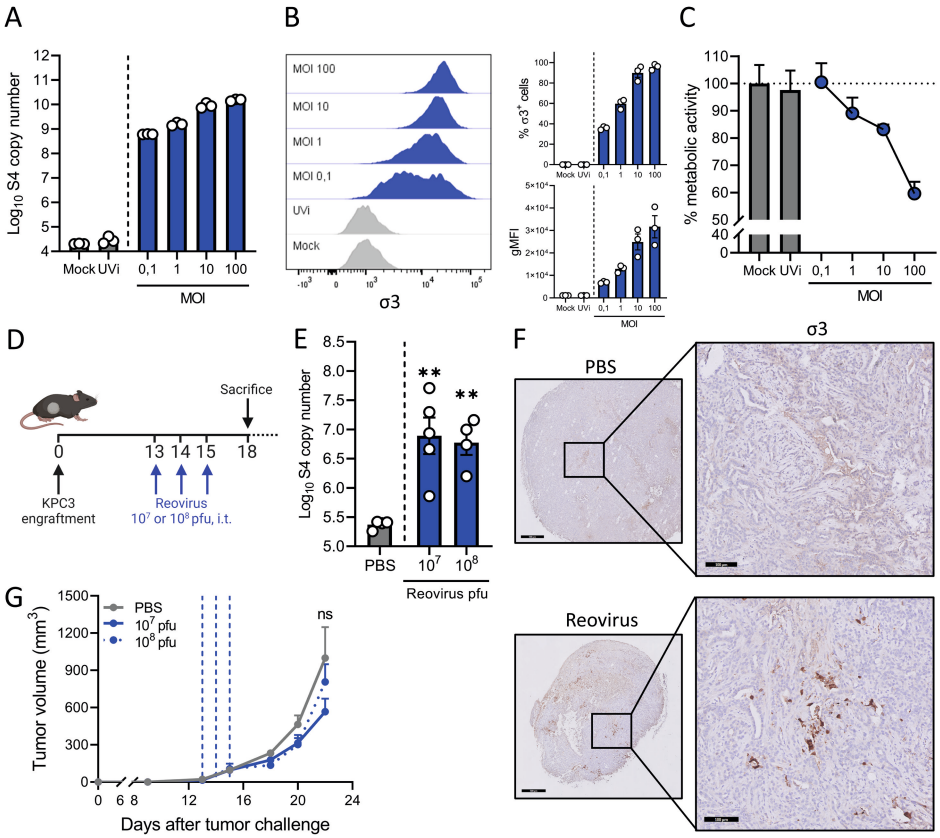

Figure 1. Reovirus efficiently replicates but does not affect tumor growth in the KPC3 pancreatic cancer model. (**A**) Numbers of reovirus S4 copies in KPC3 cells after reovirus infection. KPC3 cells (125.000/well) were infected with increasing MOIs of reovirus, PBS (Mock), or UVi (equal number of viral particles as MOI 100) as controls. Samples (n=3) were harvested 24 hours after infection and reovirus genomic RNA segment 4 (S4) copy numbers were determined by RT-qPCR. (**B**) Frequency of σ3-positive KPC3 cells 48 hours after infection with increasing MOIs of reovirus, or PBS (Mock) or UVi reovirus as controls, analyzed by flow cytometry. Bar graphs represent mean±SEM of triplicates. (**C**) Analysis of the oncolytic activity of reovirus. KPC3 cells (5000/well) were plated and infected with reovirus or controls. Metabolic activity was determined 48 hours after infection. Data represent mean±SEM of triplicates. (**D**) Design of experiment described in E-G. Mice (n=4-6/group) with established KPC3 tumors were treated with intratumoral injections of 10^7 or 10^8 pfu of reovirus on three consecutive days. PBS was used as a control. (**E**) Three days after the last reovirus injection, tumors were harvested and reovirus S4 copy numbers were determined in tumor lysates by RT-qPCR. (**F**) Representative images obtained from immunohistochemical staining of tumors for σ3. Shown are tumors treated with PBS or reovirus 10^7 pfu. Scale bars equal 500 µm and 100 µm for overview and magnification, respectively. (**G**) Mean tumor volumes after treatment with PBS or reovirus 10^7 or 10^8 pfu. Dashed vertical lines indicate days of injections. Data are presented as mean±SEM (n=4-6/group). Significance versus PBS treatment in figures E and G is determined using an ordinary one-way ANOVA with Dunnett's post-hoc test. Significance levels: ns=not significant and **p<0.01. MOI, multiplicities of infection; UVi, UV-inactivated; pfu, plaque-forming units.

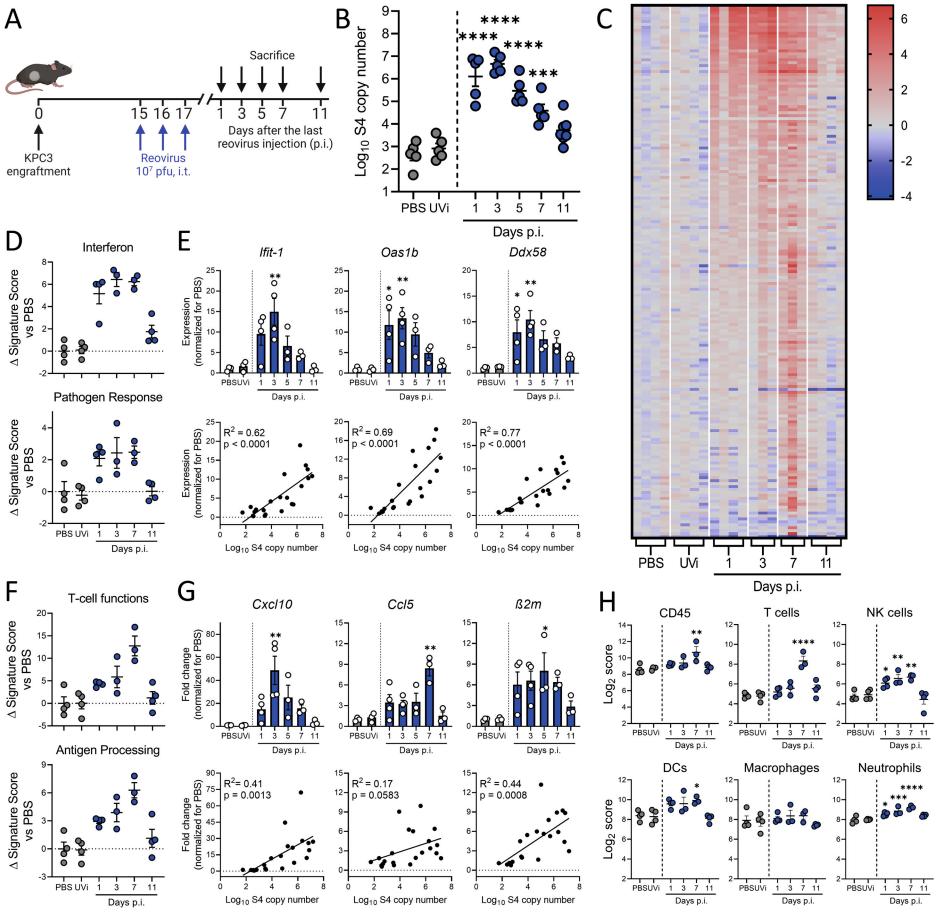

Figure 2. Replication-competent reovirus induces a potent interferon response in the tumor. (**A**) Design of the experiment described in figures B-H. Mice (n=5/group) with established KPC3 tumors were intratumorally injected with 10^7 pfu of reovirus on three consecutive days. PBS or UVi were used as controls and were harvested 3 days after the last injection. (**B**) Tumors were harvested at designated days after reovirus injection (p.i.) and viral S4 copy numbers were determined in tumor lysates by RT-qPCR. (**C**) Heatmap of all genes that were differentially expressed in the tumor (n=3-4/group) on any day after reovirus treatment (FDR $p < 0.1$ and fold change > 2 compared to PBS), as analyzed by NanoString. (**D**) Changes in signature scores on indicated days after reovirus treatment. All scores are normalized for the average score of PBS. (**E**) Relative expression of interferon response genes (upper panel) as determined by RT-qPCR, and the correlation between expression and reovirus S4 copy numbers (lower panel). (**F**) Changes in signature scores on indicated days after reovirus treatment. All scores are normalized for the average score of PBS. (**G**) Relative expression of genes involved in T-cell attraction and antigen processing (upper panel) as determined by RT-qPCR, and the correlation between expression and reovirus S4 copy numbers (lower panel). (**H**) Kinetics of specific cell type scores after reovirus treatment. All data are presented as mean±SEM. Significance versus PBS treatment is determined using an ordinary one-way ANOVA with Dunnett's post-hoc test. Correlation is determined using Pearson's correlation tests. Significance levels: *p<0.05, **p<0.01, ***p<0.001, and ****p<0.0001. Pfu, plaque-forming units; UVi, UV-inactivated reovirus.

Analysis of gene expression signatures roughly revealed two patterns: an early expressed profile, including pathways such as 'interferon' and 'pathogen response', peaking at day 1 to 5, and a late expressed profile, with pathways such as 'T-cell functions' and 'antigen processing', which peaked at day 7 (**Figure 2D-G and Figure S2B**). Expression of early interferon response genes was validated for some prime examples such as *Ifit-1, Oas1b,* and *Ddx58* using RT-qPCR (**Figure 2E**). These antiviral genes were strongly upregulated after treatment with replication-competent reovirus, but not UVi, and expression levels correlated strongly ($R^2 > 0.6$) and significantly ($p < 0.0001$) with the number of viral copy numbers in the tumor (**Figure 2E**). We also validated the expression of some genes involved in the late pathways (**Figure 2F**), such as T-cell-attracting chemokines *CxclL10, Ccl5,* and MHC class I component *β2M*, and observed increased expression levels after reovirus, but not UVi treatment (**Figure 2G**). The expression levels of these genes also significantly correlated with the number of viral copies present in the tumor, although to a lesser extent ($R^2 < 0.5$) than the early induced genes. Lastly, we analyzed the kinetics of NanoString-defined cell type scores in our dataset (**Figure 2H**). A marginal increase in CD45 score was observed on day 7, and when lineage-specific scores were examined, the score for T cells (identified by expression of *Cd3g*, *Cd3e*, *Cd3d,* and *Sh2d1a*) was most significantly upregulated at day 7 after reovirus treatment. Interestingly, natural killer (NK) cells, dendritic cells (DCs), and neutrophil scores were also enhanced on day 7. Macrophage score remained largely unaffected by reovirus treatment. Overall, we observed that reovirus replication induced a potent interferon response, including highly increased expression of inflammatory genes and T-cell-attracting chemokines.

Replication-competent reovirus recruits virus-specific T cells to the tumor

To validate that the reovirus-induced inflammatory response increased tumor infiltration by immune cells, we analyzed the cellular composition of the TME by flow cytometry and immunohistochemistry (IHC) (**Figure 3 and Figure S3**). Interestingly, the total number of $CD45^+$ immune cells in the reovirus-treated tumors was hardly altered (**Figure 3A**). However, the percentage of $CD3^+$ T cells within the $CD45^+$ population was significantly increased after reovirus administration, starting 5 days after the last reovirus injection (**Figure 3B**). This effect was replication-dependent since UVi reovirus treatment failed to increase the intratumoral T-cell density (**Figure 3B and Figure S4A**). Within the $CD3^+$ T-cell population, the $CD8^+$ T cells were significantly more enriched compared to the $CD4^+$ T cells, as seen by a significantly increased $CD8^+/CD4^+$ ratio (**Figure 3C-D**). In the tumors of reovirus-injected mice, the presence of $CD8^+$ T cells could be observed in both the border and the interior of tumors (**Figure 3E**)**.**

To gain a broader view of the TME, we performed a high-dimensional flow cytometric analysis of the lymphoid and myeloid cell compartments in the tumors 5 days after reovirus administration (**Figure 3F and Figure S4B-G**). This analysis confirmed the increased contribution of $CD8^+$ T cells (a 2,6-fold increase compared to PBS), as the total $CD45^+$ immune infiltrate increased only 1,4-fold (**Figure S4B**).

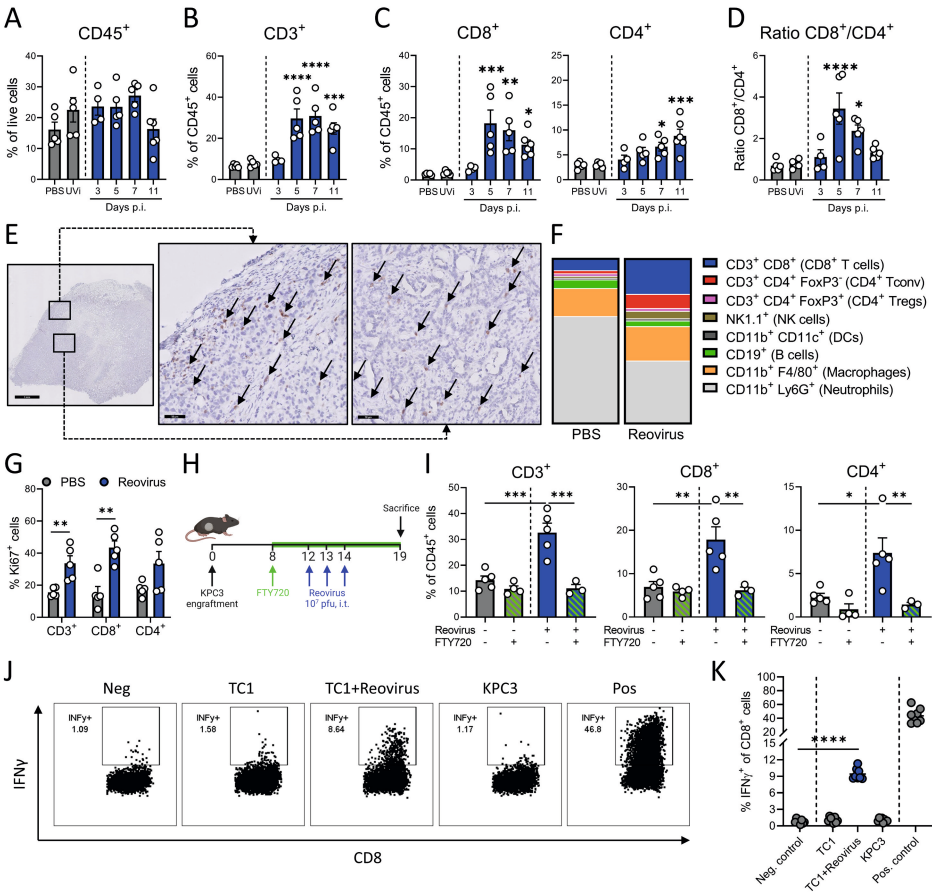

Figure 3. Replication-competent reovirus recruits virus-specific T cells to the tumor. (**A**) Frequency of CD45⁺ immune cells in the tumor on indicated days after reovirus or UVi treatment (n=5/group). (**B**) Frequency of CD3⁺ T cells within CD45⁺ immune cells in the tumor. (**C**) Frequency of CD8⁺ and CD4⁺ T cells within CD45⁺ immune cells in tumors after reovirus treatment. (**D**) Ratio between intratumoral CD8⁺ and CD4⁺ T cells. (**E**) Representative images obtained from immunohistochemical staining of tumors for CD8 (light brown). Arrows indicate CD8⁺ T cells. Scale bars equal 1 mm and 50 µm for overview and magnification, respectively. (**F**) Composition of CD45⁺ immune infiltrate in the tumor, 5 days after reovirus treatment. (**G**) Frequency of Ki67⁺ cells within CD3⁺, CD8⁺, and CD4⁺ T-cell populations in the tumor. (**H**) Design of experiment described in I. Mice (n=3-5/group) with established KPC3 tumors were intratumorally injected with reovirus (10^7 pfu) on three consecutive days and were treated with FTY720 (2,5 µg/mL FTY720 in drinking water and daily oral administration of 2 µg/g body weight). (**I**) Frequency of CD3⁺, CD8⁺, and CD4⁺ T-cell populations in the tumor. (**J**) Representative flow cytometry plots for the frequency of IFNγ⁺ cells within the intratumoral CD8⁺ T-cell population 7 days after reovirus treatment. Single-cell suspensions from tumor samples (n=8/group) were cocultured with indicated targets for six hours. Medium was used as negative (Neg.) and PMA/ionomycin was as positive (Pos.) controls, respectively. (**K**) Quantification of IFNγ⁺ cells within CD8⁺ T-cell population. See next page for continuation of figure legend. All data are presented as mean±SEM. Statistical tests used: Panels A-D: ordinary one-way ANOVA with Dunnett's post-hoc test. Panel G: Multiple unpaired t tests. Panel I: ordinary one-way ANOVA with Tukey's post-hoc test. Panel K: unpaired t test between Neg. control and TC1+Reovirus. Significance levels: *p<0.05, **p<0.01, ***p<0.001, and ****p<0.0001. UVi, UV-inactivated reovirus.

The frequency of NK cells and CD4 cells also significantly increased, and within the CD4$^+$ T-cell population, the frequency of FoxP3$^+$ CD4$^+$ regulatory T cells dramatically dropped from 40% to 10% (**Figure S4C, D**). This resulted in an enhanced ratio of CD8$^+$ cytotoxic T cells to FoxP3$^+$ regulatory T cells in the TME (**Figure S4E**). Additionally, reovirus induced activation of T cells, as indicated by increased expression of activation marker CD44 and loss of adhesion marker CD62L (**Figure S4F**). Interestingly, we observed a large population of neutrophils (CD11b$^+$Ly6G$^+$) in untreated KPC3 tumors, the frequency of which dramatically decreased after reovirus administration (**Figure S4G**). Other myeloid cell lineages, such as macrophages (CD11b$^+$ F4/80$^+$) and CD11c$^+$ macrophages (CD11b$^+$ CD11c$^+$) remained unaffected (**Figure S4G**). Overall, these analyses revealed that replication-competent reovirus converts an immunologically cold tumor-microenvironment with low T-cell infiltration into a site with a strongly enhanced abundance of activated effector T cells and NK cells and reduced frequency of neutrophils and immunosuppressive regulatory T cells.

Next, we investigated the mechanism underlying the increased T-cell density in the tumor after reovirus administration. First, we assessed the proliferation of T cells by measuring the frequency of intratumoral Ki67$^+$ T cells (**Figure 3G**). The fraction of Ki67$^+$ T cells was significantly increased after reovirus treatment, especially in CD8$^+$ T cells. We subsequently examined if the increased T-cell frequencies were solely the result of local proliferation in the tumor or were the result of increased attraction to the tumor. To this end, T-cell egress from lymph nodes was blocked with FTY720 during this experiment (**Figure 3H, I and Figure S4H, I**) (32). Interestingly, the reovirus-induced increase in intratumoral CD3$^+$ T cells, both CD4$^+$ and CD8$^+$ subsets, was completely abrogated under FTY720 conditions, whereas the abundance of total CD45$^+$ immune cell infiltrate into the tumor was not affected.

Finally, we examined the specificity of the tumor-infiltrating CD8$^+$ T cells. Tumor-infiltrating lymphocytes were cocultured for 6 hours with KPC3 tumor cells, MHC class I-matched control TC-1 tumor cells, or TC-1 cells infected with reovirus (**Figure 3J, K**). No tumor-specific response to KPC3 could be detected, but 10% of the CD8$^+$ T cells responded to reovirus-infected TC1 cells by producing IFNγ. This population of reovirus-specific T cells was specifically enriched at the site of the tumor since their frequencies were around 1% in the spleen (**Figure S4J**). We concluded that reovirus replication in the tumor leads to strong recruitment of proliferating and activated type 1 T cells, which are reovirus-specific.

Combination treatment of reovirus and CD3-bsAbs induces strong tumor regression of established TRP1-expressing tumors

The observation that reovirus replication ignites a strong influx of T cells in the otherwise immunologically cold KPC tumors provided a strong rationale to evaluate the combination of reovirus with CD3-bsAb therapy. C57BL6/J mice with palpable TRP1-expressing KPC3 tumors were treated intratumorally with reovirus and 4 days later,

when the inflammatory response had reached its full potential, CD3xTRP1 bsAbs were systemically administered (**Figure 4A**). This combination resulted in striking tumor regressions, which started directly after the first bsAb injection, whereas bsAbs or reovirus monotherapy hardly showed any tumor growth delay (**Figure 4B and Figure S5A**). Visualizing the relative change in tumor size after the start of bsAb injection indicated that combination therapy induced tumor regressions in all treated mice, whereas tumors treated with CD3xTRP1 bsAb monotherapy all increased in size (**Figure 4C**). Mice receiving the combination treatment had significantly lower tumor volumes on day 21 (**Figure 4B**) and survived significantly longer (**Figure 4D**) compared to PBS or both monotherapies.

Despite the striking regressions induced by the combination therapy, durable responses were not observed, and all tumors eventually escaped immune control (**Figure 4B-D and Figure S5A**)**.** This escape could not be prevented by an additional treatment round of reovirus and CD3xTRP1 bsAbs (**Figure S5B, C**), or by the addition of checkpoint blockade using αPD-L1 (**Figure S5D-F**). We aimed to explain the escape mechanism and first assessed T-cell presence in end-stage tumors. Immunohistochemical analysis of these samples indicated that $CD3^+$ T cells were still abundantly present in tumors from combination-treated animals (**Figure S6A**). Flow cytometry analysis confirmed the increased presence of mainly $CD8^+$ T cells in the tumors that were treated with reovirus and bsAb (**Figure S6B**) and additionally revealed that most of these T cells still displayed an activated phenotype with high expression of CD44 and an absence of CD62L (**Figure S6C**)**.** Furthermore, no striking differences in the expression of checkpoint molecules PD1, Tim3, and NKG2A were observed between T cells from the combination group and T cells from the bsAb group (**Figure S6C**)**.** These data indicated that the observed tumor escape could not be explained by the absence or exhaustion of intratumoral T cells.

We then looked at tumor-intrinsic factors and analyzed the presence of surface $TRP1^+$ cells within the $CD45^-$ tumor cell population (**Figure 4E, F and Figure S6D**). Importantly, we found that TRP1 expression was lost in nearly all tumor cells after combination treatment, versus 40% in tumors treated with bsAb alone and <20% of cells in the other groups (**Figure 4E, F**). These data imply that the robust immune pressure of combination treatment initially resulted in striking tumor regressions, but also promoted the selective expansion of TRP1-negative tumor cell clones that are insensitive to CD3xTRP1 bsAb targeting. The TRP1 protein was selected as a model antigen in this study, however, it is not an essential molecule for cell growth or survival and could therefore be lost without consequences for tumor growth. We concluded that this combination therapy led to the complete eradication of TRP1-expressing tumor cells, concomitantly leading to the escape of tumor variants that lost the targeted antigen.

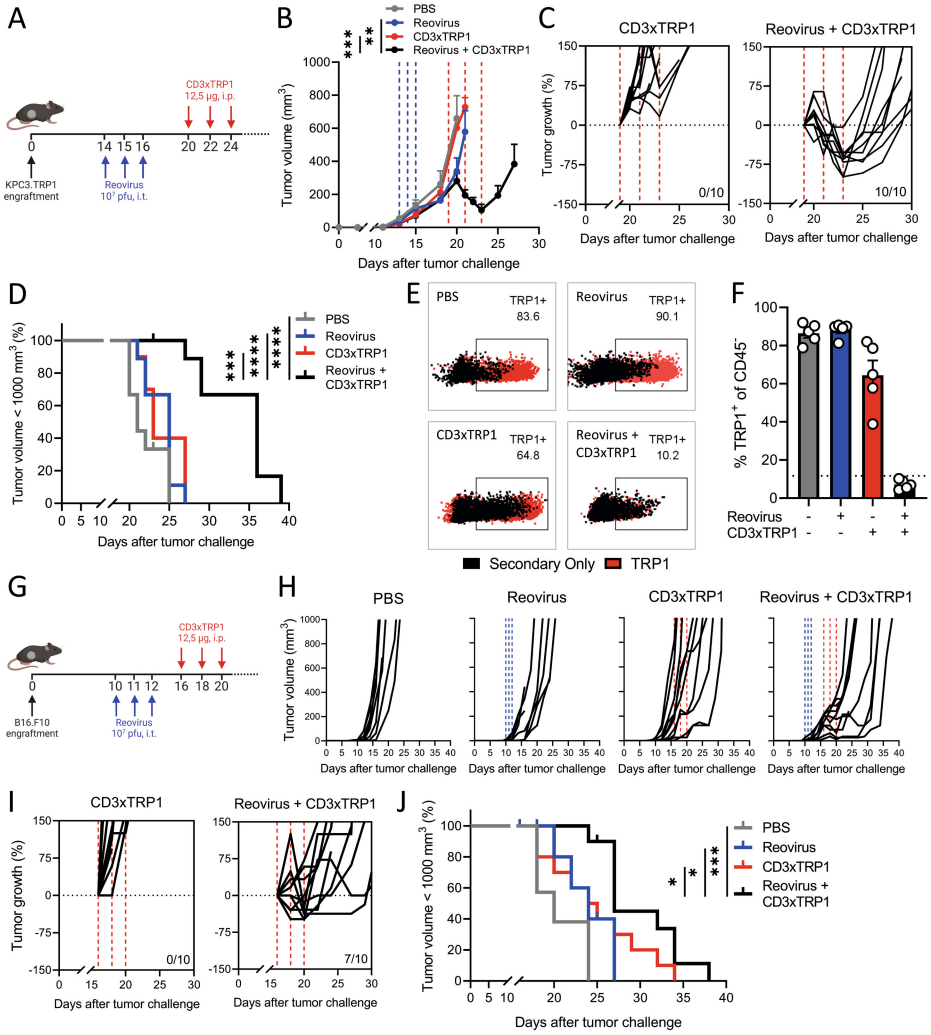

Figure 4. Combination treatment of reovirus and CD3xTRP1 bsAbs induces regression of established TRP1-expressing tumors. (**A**) Design of experiment described in figures B-F. Mice (n=8-10/group) with established KPC3.TRP1 tumors were intratumorally injected with reovirus (10^7 pfu) on three consecutive days. After 4 days, mice received intraperitoneal injections of 12,5 µg CD3xTRP1 bsAbs (CD3xTRP1) or PBS as control. (**B**) Average tumor growth curves±SEM. Dashed lines indicate the timing of injection with Reovirus (blue) or CD3xTRP1 (red). Differences in mean tumor volumes versus Reovirus + CD3xTPR1 treatment on day 21 are determined by one-way ANOVA with Dunnett's post-hoc test. (**C**) Relative changes in tumor volume of individual mice from the start of CD3xTRP1 bsAb treatment. Indicated is the number of mice with tumor regressions. (**D**) Kaplan-Meier survival graphs of mice in indicated treatment groups. (**E**) Overlayed dot plots indicating the percentage of TRP1⁺ cells on representative tumors of each group. Black dots show background staining of secondary antibody. Red dots show staining using primary αTRP1 antibody followed by the secondary antibody. (**F**) Quantification of TRP1 expression. Dashed line indicates the mean background staining of secondary antibody. Data represent mean±SEM. (**G**) Design of experiment described in figures H-J. Mice (n=8-10/group) with established B16.F10 tumors were intratumorally injected with reovirus (10^7 pfu) on three consecutive days. After 4 days, mice received intraperitoneal injections of 12,5 µg CD3xTRP1 bsAbs or PBS as control.

>>

>> (**H**) Individual growth curves of B16.F10-bearing mice receiving indicated treatments. (**I**) Relative changes in tumor volume from the start of CD3xTRP1 bsAb treatment. Indicated is the number of mice with tumor regressions. (**J**) Kaplan-Meier survival graphs of mice in indicated treatment groups. Log-rank test was used to compare differences in survival. Significance levels: *p<0.05, **p<0.01, ***p<0.001, and ****p<0.0001. Pfu, plaque-forming units; bsAbs, bispecific antibodies.

To demonstrate the efficacy of this combination treatment in another immunologically cold tumor model, we employed the murine melanoma model B16.F10 (33), which spontaneously expresses the melanocyte-lineage antigen TRP1. Although all B16.F10 cells expressed TRP1 on their cell surface, the level of expression in B16.F10 was a magnitude lower compared to KPC.TRP1 (**Figure S7A**). In vitro, reovirus was able to efficiently replicate in B16.F10 cells, however, the number of viral copy numbers and the frequency of $\sigma3^+$ cells were lower compared to KPC3 (**Figure S7B, C**). Interestingly, despite viral replication in B16.F10 cells, oncolysis hardly occurred, even at a MOI of 100 (**Figure S7D**). *In vivo,* reovirus was able to efficiently replicate (**Figure S7E**) and to increase the T cell density in established subcutaneous B16.F10 tumors after intratumoral injection (**Figure S7F**). Earlier, we reported that CD3xTRP1 significantly delayed tumor growth in B16.F10 tumors, when given early after tumor challenge (25). Similar to the KPC3.TRP1 model, the combination regimen of reovirus and CD3xTRP1 was required to induce tumor regressions in established B16.F10 tumors (**Figure 4G, H**). Whereas CD3xTRP1 monotherapy delayed tumor growth in some animals (**Figure 4H**), therapy-mediated tumor regressions were exclusively found in 7 out of 10 animals of the combination group (**Figure 4I**). The combination treatment also significantly prolonged survival (**Figure 4J**).

The combination of reovirus and CD3-bsAbs is effective in a human, orthotopic HER2⁺ breast cancer model

Additionally, we aimed to investigate the efficacy of the combination of reovirus and CD3-bsAbs in a more clinically relevant setting. We employed the human epidermal growth factor receptor (HER2) positive breast cancer model BT474 (34), as a close-to-patient model to test CD3xHER2 bsAb therapy. BT474 cells express high levels of HER2 and were susceptible to reovirus replication (**Figure 5A, B**). BT474 tumors were engrafted orthotopically in the fourth mammary fat pad of NSG mice, and human PBMCs were intravenously administered as a source of effector cells before reovirus and bsAb administration (**Figure 5C**). In contrast to our experiments in immunocompetent mice, reovirus alone already showed some efficacy by impairing tumor growth (**Figure 5D**). Whereas CD3xHER2 monotherapy had no therapeutic efficacy in comparison to the PBS-treated group, the combination of reovirus with CD3xHER2 bsAbs induced strong tumor regressions in all animals (**Figure 5D**) and a significant average tumor shrinkage calculated from the moment of PBMC injection (**Figure 5E**). Collectively, these results show that the efficacy of bsAb therapy in immunologically cold, solid tumors such as KPC3, B16.F10, and BT474 can be greatly enhanced by prior sensitization with reovirus.

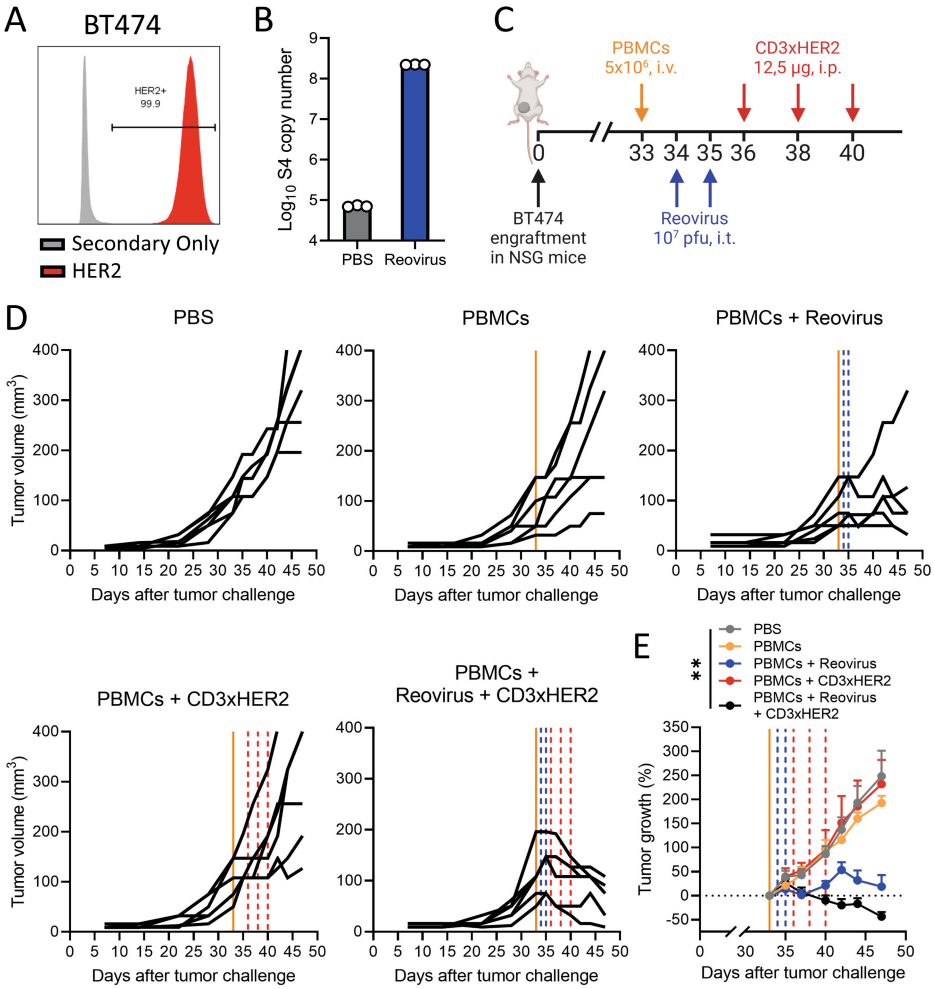

Figure 5. Combination of reovirus and CD3-bsAbs is effective in a human, orthotopic HER2⁺ breast cancer model. (**A**) HER2 expression percentages on BT474 cells, as analyzed by flow cytometry using a 2-step protocol. (**B**) Number of reovirus S4 copies in BT474 cells after reovirus infection. BT474 cells (200.000/well) were infected with reovirus MOI 10 or PBS (Mock) as a control. Samples (n=3) were harvested 24 hours after infection and the number of viral S4 copies was determined by RT-qPCR. (**C**) Design of experiment described in figures D-E. Mice (n=6/group) with established BT474 tumors were intravenously injected with $5x10^6$ human PBMCs, and thereafter intratumorally injected with reovirus (10^7 pfu) on two consecutive days. After 4 days, mice received intraperitoneal injections of 12,5 µg CD3xHER2 bsAbs (CD3xHER2) or PBS as control. (**D**) Individual growth curves of BT474-bearing mice receiving indicated treatments. Lines indicate the timing of injection with PBMCs (orange), Reovirus (blue), or CD3xHER2 (red). (**E**) Average relative changes (±SEM) in tumor volume from the start of CD3xHER2 bsAb treatment. Significance versus PBS on day 42 was calculated using one-way ANOVA with Dunnett's post-hoc test. Significance level: **p<0.01. MOI, multiplicities of infection; bsAbs, bispecific antibodies.

Treatment sequence is important for the synergistic effect of the reovirus and CD3-bsAb combination therapy

Here, we used two separate treatment modalities applied sequentially, but alternatively, genes coding for T-cell-engaging antibodies can also be introduced into oncolytic viruses as transgenes (35). For this reason, we investigated whether timing was important for the observed synergistic effect and if comparable tumor regressions could also be observed if reovirus and CD3xTRP1 bsAbs were administered simultaneously or in reversed order (**Figure 6**). Interestingly, steady tumor growth without any regressions was observed when we switched the sequence of treatment arms and first administered bsAbs (**Figure 6A, D**). Simultaneous administration of bsAb on the day of reovirus injection did induce regressions in tumor volume, but tumors started to regrow fast (**Figure 6B, D**).

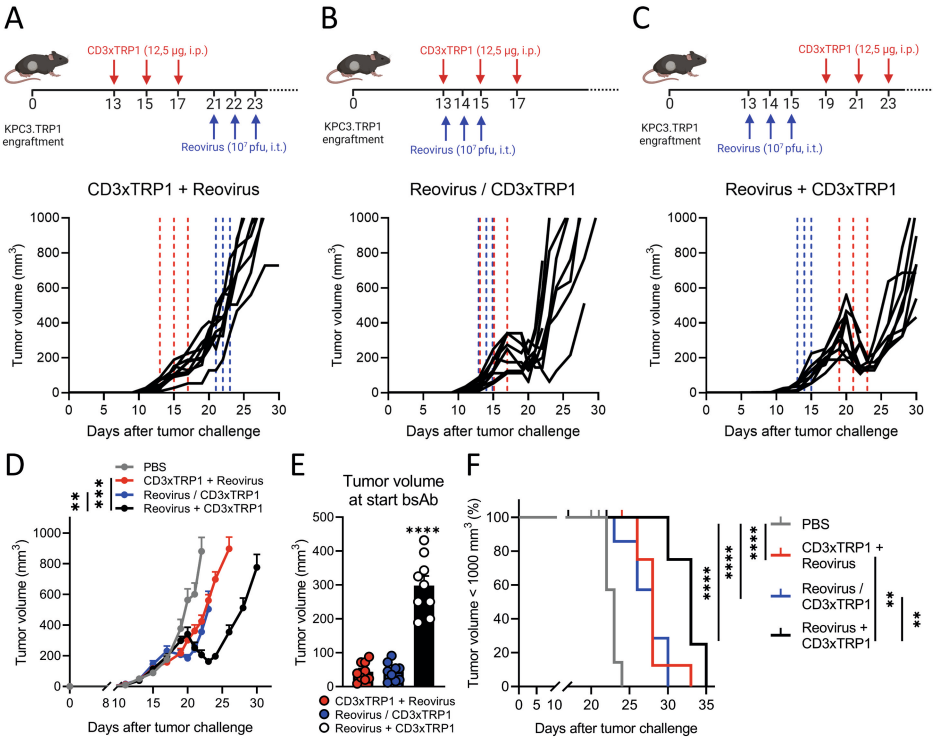

Figure 6. Treatment sequence is important for the synergistic effect of the reovirus and CD3-bsAb combination therapy. Treatment schedule and individual tumor growth curves of mice (n=8-10/group) that received intraperitoneal injections (12,5 µg/mouse) of CD3xTRP1 bsAbs before (**A**), simultaneously with (**B**) or after (**C**) intratumoral reovirus injections (10^7 pfu/mouse). Dashed vertical lines indicate the timing of injection with Reovirus (blue) or CD3xTRP1 (red). (**D**) Average tumor growth curves (±SEM) of experimental groups shown in A-C compared to PBS treatment. Significance versus Reovirus + CD3xTPR1 treatment on day 23 is determined by comparing tumor volumes using a one-way ANOVA with Dunnett's post-hoc test. (**E**) Mean±SEM tumor volume at the start of CD3xTRP1 bsAb treatment for treatment schedules CD3xTRP1 + Reovirus (day 13), Reovirus/CD3xTRP1 (day 13), and Reovirus + CD3xTRP1 (day 19). Ordinary one-way ANOVA with Tukey's post-hoc test was used to compare means.

>>

>> (**F**) Kaplan-Meier survival curves of mice in different treatment schedules. Log-rank test was used to compare differences in survival. Significance levels: *p<0.05 and **** p<0.0001. Pfu, plaque-forming units; bsAbs, bispecific antibodies.

Our previous regimen of reovirus before bsAbs led to significantly smaller tumor volumes on day 23 after the tumor challenge, indicating more durable and deeper regressions compared to the other regimens (**Figure 6C, D**). Importantly, simultaneous treatment with reovirus and bsAbs did induce small regressions, but these occurred when tumor volumes were still relatively low at the start of bsAb treatment (**Figure 6E**). In contrast, pre-treatment with reovirus caused tumors to undergo steeper regressions, even though the tumor volume was significantly higher at the start of bsAb treatment. All combination treatment regimens significantly improved survival in comparison to the untreated group, but the exploitation of reovirus as a preconditioning regimen performed significantly better compared to both other schedules (**Figure 6F**). In conclusion, these data highlight the importance of sensitization of tumors with reovirus preceding bispecific antibody treatment to optimally harness the full potential of this combination.

Intratumorally injected reovirus sensitizes local and distant cold tumors for subsequent treatment with CD3xTRP1 therapy

In previous experiments, we observed that intratumoral delivery of reovirus also induced systemic activation of both $CD8^+$ and $CD4^+$ T cells in the spleen, reflected by increased expression of CD44, KLRG1, and PD1, and absence of adhesion molecule CD62L (**Figure 7A**). To evaluate the possible systemic effects of local reovirus administration, a bilateral tumor model was used. Mice were engrafted with a subcutaneous KPC3 tumor on the right flank and one week later received another tumor on the left flank (**Figure 7B**). After reovirus treatment, we assessed the presence of reovirus copy numbers in both the injected (local) and the non-injected (distant) tumor. To our surprise, we detected a significantly increased number of viral genomic copies in the distant tumor after reovirus treatment, although at lower numbers than in the injected tumor (**Figure 7C**). Interestingly, no increase in reovirus copy numbers could be observed in other organs except for the tumor-draining lymph node (TDLN) (**Figure 7D**). The presence of reovirus in the distant tumor also led to an increased expression of a selection of ISGs (**Figure 7E**) and a subsequent increased influx of $CD8^+$ T cells, indicating that locally injected reovirus can find its way to distant tumors, and is associated with the recruitment of immune cells there (**Figure 7F**). We then investigated whether our combination treatment could also effectively control the growth of distant tumors. As expected, monotherapy with CD3xTRP1 bsAbs did not affect the tumor growth of local or distant tumors (**Figure 7G**). Strikingly, combination treatment also induced regression of the distant KPC3.TRP1 tumors (**Figure 7H**). This effect was TRP1-targeted since no regressions were observed in distant tumors not expressing TRP1 (KPC3). These findings suggest that the combination of reovirus and CD3-bsAbs might also be effective in metastatic disease.

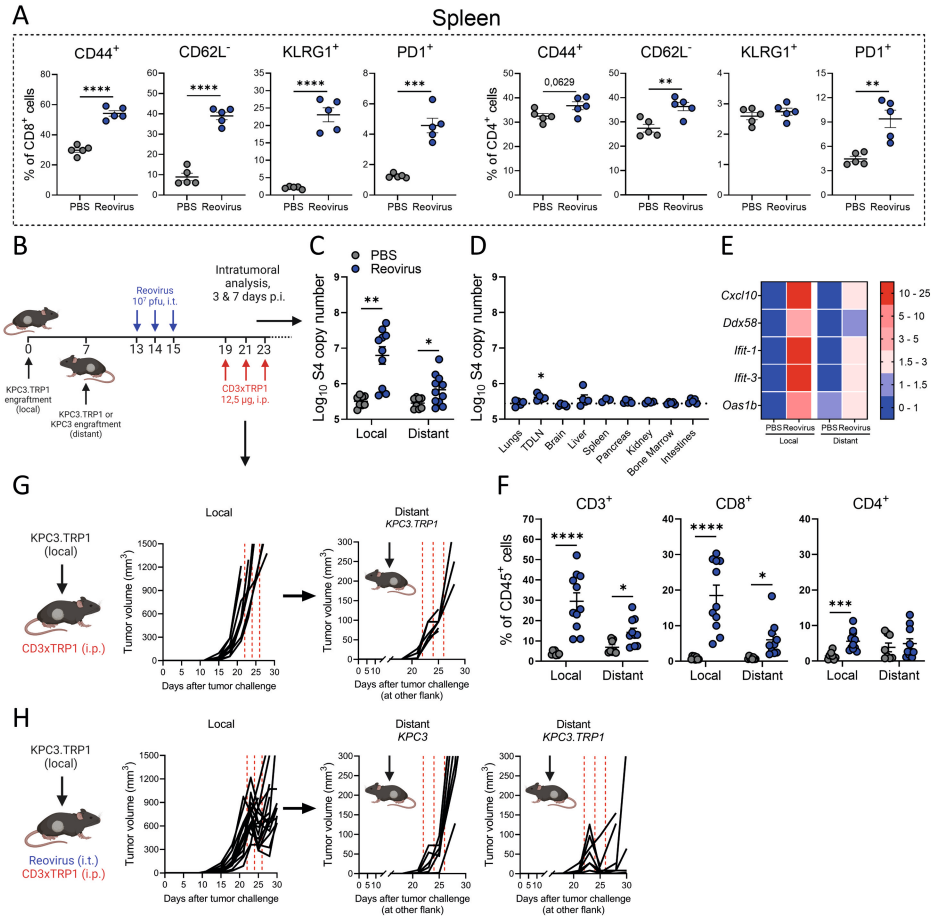

Figure 7. Intratumorally injected reovirus sensitizes local and distant cold tumors for subsequent treatment with CD3xTRP1 therapy. (**A**) Expression of activation markers on splenic CD8⁺ or CD4⁺ T cells 5 days after reovirus or PBS administration (n=5/group). (**B**) Treatment schedule of experiment described in C-G. Mice (n=8-10/group) were subcutaneously inoculated with KPC3.TRP1 cells in the right flank. Seven days later, another KPC3.TRP1 or KPC3 tumor was inoculated in the left flank. Mice received intratumoral injections of reovirus (10^7 pfu) in the primary right tumor. Then, mice were sacrificed for intratumoral analysis at 3 and 7 days after the last reovirus injection (panels C-F; pooled results of 2 independent experiments with similar results) or mice received subsequent intraperitoneal injections of 12,5 µg CD3xTRP1 bsAbs and tumor size was monitored (panels G and H). (**C**) S4 copy numbers in local and distant tumors 3 days after reovirus treatment or PBS as control. (**D**) S4 copy numbers present in other organs of reovirus-treated mice 3 days after reovirus administration. Dashed horizontal line represents average S4 copy numbers in PBS-treated mice. (**E**) Heatmap of relative expression of interferon response genes in the local and distant tumors as determined by RT-qPCR. Numbers indicate fold change versus PBS-treated local tumors. (**F**) Frequency of T cells in local and distant tumors of mice 7 days after local reovirus administration. Data presented as mean±SEM. Differences between PBS and reovirus in panels A and C-F were determined with unpaired t tests. (**G**) Individual tumor growth curves of local and distant tumors of mice (n=8/group) treated with CD3xTRP1. Dashed red lines indicate the timing of injection.

>>

>> (**H**) Individual tumor growth curves of local and distant TRP1-expressing (KPC3.TRP1) or WT KPC3 tumors of mice after intratumoral treatment with reovirus and subsequent intraperitoneal injections with CD3xTRP1. Dashed lines indicate the timing of injection with Reovirus (blue) or CD3xTRP1 (red). Significance levels: *p<0.05, **p<0.01, ***p<0.001, and ****p<0.0001. Pfu, plaque-forming units; bsAbs, bispecific antibodies.

Intravenous administration of reovirus is also effective in preconditioning the tumor microenvironment

In the present study, reovirus was injected intratumorally to ensure efficient delivery at the tumor site. However, in most clinical studies, intravenous infusion of reovirus has been applied (36) and effective delivery to tumor sites, including the brain, was demonstrated (11). Therefore, we tested the therapeutic efficacy of systemic delivery of reovirus (**Figure 8A**). Intravenous administration of 10^7 and 10^8 pfu/injection resulted in detectable numbers of reovirus genomic copies in the tumor, although in significantly lower numbers compared to intratumoral administration of 10^7 pfu of reovirus (**Figure 8B**). Increased expression of a selection of ISGs was observed in comparison to the PBS group (**Figure 8C**), suggesting that intravenously administered reovirus can induce an interferon response in the TME. Intravenous administration of reovirus was effective as a preconditioning method since tumor outgrowth was temporarily halted, but no regressions were observed as was the case after intratumoral administration (**Figure 8D-F**)**.** Mice treated with any of the combination treatments had smaller tumor volumes (**Figure 8E**) and significantly prolonged survival times (**Figure 8F**) in comparison to the untreated group. These data imply that preconditioning of the TME with both intravenous and local administration of reovirus is effective to turn CD3-bsAbs into a potent immunotherapy for solid cancers. Collectively, our data demonstrate that replication-competent reovirus turns an otherwise unsuccessful CD3-bsAb therapy into a powerful systemic treatment.

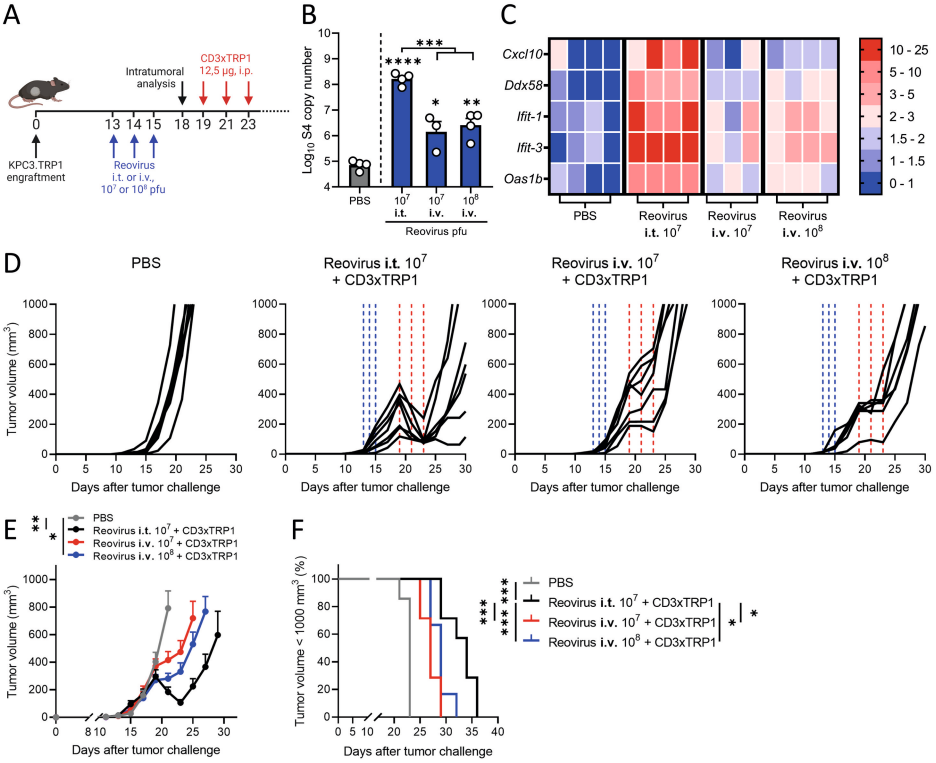

Figure 8. Intravenous administration of reovirus is also effective in pre-conditioning the tumor microenvironment. (**A**) Design of experiment described in figures B-F. KPC3.TRP1-bearing mice were intratumorally or intravenously injected with reovirus (10^7 or 10^8 pfu) on three consecutive days. Tumors were harvested 3 days after the last reovirus injection for intratumoral analysis (n=3-4/group), or mice received intraperitoneal injections of 12,5 µg CD3xTRP1 bsAbs (CD3xTRP1) or PBS as control (n=6-7/group). (**B**) Viral S4 copy number in tumor lysates by RT-qPCR. Mean±SEM. (**C**) Heatmap of relative expression of interferon response genes in tumors versus PBS treatment, as determined by RT-qPCR. (**D**) Individual tumor growth curves of KPC3.TRP1-bearing mice (n=6-8/group) that were intratumorally or intravenously injected with reovirus (10^7 or 10^8 pfu) on three consecutive days. After 4 days, mice received intraperitoneal injections of 12,5 µg CD3xTRP1 bsAbs (CD3xTRP1) or PBS as control. Dashed vertical lines indicate the timing of injection with Reovirus (blue) or CD3xTRP1 (red). (**E**) Average±SEM tumor growth curves. Differences in mean tumor volumes versus PBS treatment on day 21 are determined by one-way ANOVA with Dunnett's post-hoc test. (**F**) Kaplan-Meier survival curves of mice. Log-rank test was used to compare differences in survival. Significance levels: *p<0.05, **p<0.01, and ****p<0.0001. Pfu, plaque-forming units; bsAbs, bispecific antibodies.

DISCUSSION

In this study, we demonstrated that preconditioning the tumor microenvironment with oncolytic reovirus is an attractive strategy to prime immunologically cold tumors for T-cell-engaging antibody therapy. Tumor-selective replication of competent reovirus converted the tumor microenvironment to an inflamed site with a strong IFN signature

and T-cell-attracting chemokines, followed by an enhanced influx of NK cells and activated T cells. Subsequent systemic administration of T-cell-engaging antibodies induced strong tumor regressions of reovirus-injected and distant non-injected lesions, implying that this strategy may be effective for the treatment of metastatic disease.

Although OVs are considered potent anticancer modalities, reovirus and several others have demonstrated limited therapeutic efficacy when used as a monotherapy. Since oncolytic activity may not be the main asset of reovirus as an anticancer therapeutic, we focused on its potential to modify the TME. RNA viruses, typically replicate with fast kinetics and induce a very potent type I interferon response (37). Indeed, our analysis of reovirus-induced immune dynamics revealed a very fast and potent induction of intratumoral interferon response, followed by a robust influx of T cells. UV-inactivated, replication incompetent reovirus did not induce an interferon gene signature and T-cell influx in the TME, although it still contains pathogen-associated molecular patterns (PAMPs) that may be recognized by pattern-recognition receptors (PRRs) (38). Although UV-inactivated reovirus has shown to be effective in the induction of tumor-specific T cells by human dendritic cells in an *in vitro* setting,(31) in our *in vivo* setting replication was required to induce a potent interferon response and subsequent T-cell infiltration into the tumor. In contrast, a modified vaccinia virus did induce intratumoral inflammation and T-cell influx after inactivation, indicating that this OV holds sufficient viral PAMPs in the absence of viral replication (39).

Intratumoral injections lead to 'islands' of reovirus production within the tumor, resulting in local amplification and release of virus particles. Concomitantly, we found viral spread in the animals from injected tumors to distant non-injected tumors, without affecting healthy tissues except for low levels in the TDLN. Previous work already showed that various cell types such as T cells, DCs, monocytes, and granulocytes can act as cellular carriers and deliver infectious reovirus particles to tumor cells, even in the context of preexisting antiviral immunity (40-42). We speculate that one of these immune cell types is involved in carrying infectious reovirus particles via the TDLN to distant tumors. Further research is required to elucidate the exact cellular carrier or if reovirus can migrate without any cellular carrier.

Local versus systemic delivery of OVs is a huge topic of debate. Local delivery of OVs is in clinical practice for T-VEC (13,43) and is used in many preclinical studies including the present study to ensure efficient delivery to the tumor site (12). However, in most clinical studies, reovirus is administered intravenously (11,36). One advantage of intravenous delivery is that it does not rely on injectable tumor lesions, which are not available in the majority of cancer types. Here, we showed that intravenously injected reovirus is able to reach the tumor and sensitize tumors for subsequent CD3-bsAb therapy. However, the antitumor efficiency of the combination with CD3-bsAbs is lower when compared to intratumorally injected reovirus. Even a ten-fold higher dose of systemically administered reovirus significantly underperformed intratumoral delivery, suggesting

that intravenous delivery would need to be improved to reach its full potential. One previously suggested method to enhance reovirus delivery is to load reovirus on the aforementioned cellular carriers (40). Nevertheless, the efficacy of the intravenously delivered reovirus in this model is an important finding since it paves the way for the clinical application of such a combination regardless of the tumor location and route of administration.

Reovirus and other OVs have already demonstrated to combine well with checkpoint blockade, a therapy that depends on the presence of tumor-specific T cells (10-12). OVs and T-cell-engaging antibody therapy is an emerging and exciting new field of research. We demonstrated that prior sensitization with reovirus greatly enhanced the efficacy of CD3-bsAb therapy in immunologically cold tumors. However, others introduced bispecific T-cell engagers (BiTE) as transgenes into OVs (44-47). For instance, treatment with oncolytic measles virus encoding CD3-BiTEs demonstrated delayed tumor growth and prolonged survival in immunocompetent C57BL/6J mice harboring subcutaneous MC38 or B16 tumors (44). Similarly, an oncolytic adenovirus engineered with a CD3xEGFR BiTE and an oncolytic vaccinia virus encoding a CD3xEPHA2 BiTE showed antitumor activity in xenograft models and an oncolytic adenovirus encoding a CD3xEpCAM BiTE was able to activate endogenous T cells kill tumor cells in primary human tumor samples of malignant peritoneal ascites and pleural exudates (45-47). Although encoding bsAbs or BiTEs in OVs has several advantages such as reduction of treatment burden for patients (35), our data imply that these strategies do not exploit the full potential of this combination therapy as the T-cell influx peaks around a week after reovirus application, when viral genomic copies start to decline. In the studies with BiTE-encoding OVs, the kinetics of expression of the transgene may not parallel the kinetics of the OV-induced T-cell activation, especially since BiTE molecules have a very short half-life due to their small size and the absence of a stabilizing Fc tail (3). Most of the T-cell engaging activity might already be declined at the peak of T-cell-attracting chemokines. We therefore advocate to separate the administration of OVs from bsAbs and consider OV injection as a preconditioning strategy. Further research is however warranted to fully understand the optimal regiment of OV and bsAb delivery, including the biodistribution of the OVs and bsAbs, and how this differs between OVs, bsAbs and even tumor types.

The mechanism of action of CD3-bsAbs is not yet completely understood. For instance, in our studies, we did not assess whether CD3xTRP1 bsAbs first bind TRP1 in the tumor and then engage T cells that are infiltrating into the tumor due to reovirus-induced inflammation, or if bsAbs bind T cells in the lymph node, spleen or the circulation and subsequently activate these T cells upon binding of TRP1 in the tumor (4). Elucidating this mode of action might be important to further harness the full potential of CD3-bsAbs as a monotherapy and in combination with OVs since it will guide future improvements in therapeutic efficacy.

Importantly, our data demonstrated that the combination of OV and CD3-bsAbs is an extremely powerful therapy that imposed a strong, immunological selective pressure on the tumors, leading to initial regressions but later on in relapsed tumors that lost expression of the antigen. We used the melanoma-associated antigen TRP1 as a well-known model antigen. This surface-expressed protein is involved in melanin production but is not essential for cell growth or survival. The use of this particular model antigen allowed us to investigate therapy resistance on the one hand, but on the other can be considered a limitation of our study. It emphasizes the importance of the careful selection of the targeted antigen when this combination strategy is translated to the clinic. For effective bsAb therapy in humans, the ideal target antigen needs to be selectively and abundantly expressed on tumor cells but should also be essential for tumorigenesis. One such target is human epidermal growth factor 2 (HER2), and we employed human CD3xHER2 as the second bsAb to demonstrate proof-of-concept of our combination strategy in the $HER2^+$ BT474 model. In this model, we observed some close-to-complete regressions, but we were not able to determine durable responses in these animals due to increasing viremia over time, which we attributed to the lack of a functional adaptive immune system in these NSG mice. Although HER2 and other classical tumor-associated antigens such as EpCAM and epidermal growth factor receptor (EGFR) represent attractive targets, they are not entirely tumor-specific. So-called 'on-target, off-tumor toxicity' might limit the therapeutic potential of these targets (48,49). Instead, targeting of highly tumor-specific antigen glypican-3 (GPC3) or the tumor-specific mutant of EGFR (EGFRvIII) showed limited and manageable toxicity, and striking antitumor efficacy in immunocompetent mouse models or patients with recurrent glioblastoma (50,51). These data illustrate that further extensive target discovery and testing are required to create safe and effective bsAbs for clinical use. The intracellular proteome might even be considered a good target for bsAbs, via surface display of tumor-specific peptide/MHC complexes (52).

Together, our data demonstrate that combined local reovirus treatment and systemic T-cell-engaging antibody therapy induces strong tumor regressions of both local and distant solid tumors. Both CD3-bsAbs and OVs are already undergoing rigorous clinical testing, suggesting a possible fast translation of our work to the clinic.

DECLARATIONS

Acknowledgments. The authors thank Lisa Griffioen, Noortje de Bie, and Marjolein Sluijter for their technical assistance, the Animal Facility of the LUMC for their excellent care of the animals, and Michael Fiebig (Absolute Antibody) for his collaboration. The hybridoma 4F2 (reovirus σ3), developed by T. S. Dermody from the University of Pittsburgh School of Medicine, was obtained from the Developmental Studies Hybridoma Bank, created by the NICHD of the NIH and maintained at The University of Iowa, Department of Biology, Iowa City, IA 52242.

Author contributions. Conceptualization, TvH and NvM; Methodology, CG, PK, DvdW, RvdO, JM, DM, RH, TvH and NvM; Formal analysis, CG, PK, DM; Investigation, CG, PK, RvdO; Resources, DvdW, RH; Writing – Original Draft, CG, TvH, NvM; Writing - Review & Editing, All authors; Visualization, CG; Supervision, SHvdB, TvH and NvM, Funding acquisition, SHvdB, TvH, and NvM. All authors approved the final version of the manuscript.

Funding. This work was financially supported by the Dutch Cancer Society Bas Mulder Award 11056 (to NvM), a PhD fellowship from Leiden University Medical Center (to CG), and the Support Casper campaign by the Dutch foundation 'Stichting Overleven met Alvleesklierkanker' (supportcasper.nl) project numbers SOAK 17.04 and 19.03.

Competing interests. None declared.

Ethics approval. All mouse studies were approved by the institutional Animal Welfare Body of Leiden University Medical Center and carried out under project licenses AVD1160020187004 or AVD116002015271, issued by the competent authority on animal experiments in the Netherlands (named CCD). Experiments were performed following the Dutch Act on Animal Experimentation and EU Directive 2010/63/EU ("On the protection of animals used for scientific purposes") at the animal facility of the Leiden University Medical Center (LUMC), The Netherlands.

Data availability statement. All data relevant to this study are included in the main text or the supplementary materials and are available on reasonable request.

REFERENCES

1. Runcie K, Budman DR, John V, Seetharamu N. Bi-specific and tri-specific antibodies- the next big thing in solid tumor therapeutics. Molecular medicine (Cambridge, Mass) **2018**;24:50
2. Bargou R, Leo E, Zugmaier G, Klinger M, Goebeler M, Knop S*, et al.* Tumor Regression in Cancer Patients by Very Low Doses of a T Cell–Engaging Antibody. Science **2008**;321:974-7
3. Labrijn AF, Janmaat ML, Reichert JM, Parren P. Bispecific antibodies: a mechanistic review of the pipeline. Nature Reviews Drug Discovery **2019**;18:585-608
4. Mandikian D, Takahashi N, Lo AA, Li J, Eastham-Anderson J, Slaga D*, et al.* Relative Target Affinities of T-Cell–Dependent Bispecific Antibodies Determine Biodistribution in a Solid Tumor Mouse Model. Molecular cancer therapeutics **2018**;17:776-85
5. Offner S, Hofmeister R, Romaniuk A, Kufer P, Baeuerle PA. Induction of regular cytolytic T cell synapses by bispecific single-chain antibody constructs on MHC class I-negative tumor cells. Molecular Immunology **2006**;43:763-71
6. Mack M, Gruber R, Schmidt S, Riethmüller G, Kufer P. Biologic properties of a bispecific single-chain antibody directed against 17-1A (EpCAM) and CD3: tumor cell-dependent T cell stimulation and cytotoxic activity. J Immunol **1997**;158:3965-70
7. Dahlén E, Veitonmäki N, Norlén P. Bispecific antibodies in cancer immunotherapy. Therapeutic advances in vaccines and immunotherapy **2018**;6:3-17
8. Herbst RS, Soria J-C, Kowanetz M, Fine GD, Hamid O, Gordon MS*, et al.* Predictive correlates of response to the anti-PD-L1 antibody MPDL3280A in cancer patients. Nature **2014**;515:563-7
9. Chen DS, Mellman I. Elements of cancer immunity and the cancer-immune set point. Nature **2017**;541:321-30
10. Groeneveldt C, van Hall T, van der Burg SH, ten Dijke P, van Montfoort N. Immunotherapeutic potential of TGF-β inhibition and oncolytic viruses. Trends in Immunology **2020**;41:406-20
11. Samson A, Scott KJ, Taggart D, West EJ, Wilson E, Nuovo GJ*, et al.* Intravenous delivery of oncolytic reovirus to brain tumor patients immunologically primes for subsequent checkpoint blockade. Science translational medicine **2018**;10
12. Bourgeois-Daigneault MC, Roy DG, Aitken AS, El Sayes N, Martin NT, Varette O*, et al.* Neoadjuvant oncolytic virotherapy before surgery sensitizes triple-negative breast cancer to immune checkpoint therapy. Science translational medicine **2018**;10
13. Ribas A, Dummer R, Puzanov I, VanderWalde A, Andtbacka RHI, Michielin O*, et al.* Oncolytic Virotherapy Promotes Intratumoral T Cell Infiltration and Improves Anti-PD-1 Immunotherapy. Cell **2017**;170:1109-19 e10
14. Mahalingam D, Goel S, Aparo S, Patel Arora S, Noronha N, Tran H*, et al.* A Phase II Study of Pelareorep (REOLYSIN(®)) in Combination with Gemcitabine for Patients with Advanced Pancreatic Adenocarcinoma. Cancers (Basel) **2018**;10:160
15. Sborov DW, Nuovo GJ, Stiff A, Mace T, Lesinski GB, Benson DM*, et al.* A Phase I Trial of Single-Agent Reolysin in Patients with Relapsed Multiple Myeloma. Clinical Cancer Research **2014**;20:5946-55
16. Duncan MR, Stanish SM, Cox DC. Differential sensitivity of normal and transformed human cells to reovirus infection. J Virol **1978**;28:444-9
17. Shmulevitz M, Marcato P, Lee PWK. Unshackling the links between reovirus oncolysis, Ras signaling, translational control and cancer. Oncogene **2005**;24:7720-8
18. Thirukkumaran CM, Nodwell MJ, Hirasawa K, Shi Z-Q, Diaz R, Luider J*, et al.* Oncolytic Viral Therapy for Prostate Cancer: Efficacy of Reovirus as a Biological Therapeutic. Cancer research **2010**;70:2435-44
19. Zhao X, Chester C, Rajasekaran N, He Z, Kohrt HE. Strategic Combinations: The Future of Oncolytic Virotherapy with Reovirus. Molecular cancer therapeutics **2016**;15:767-73
20. van den Wollenberg DJM, Dautzenberg IJC, van den Hengel SK, Cramer SJ, de Groot RJ, Hoeben RC. Isolation of reovirus T3D mutants capable of infecting human tumor cells independent of junction adhesion molecule-A. PLoS One **2012**;7:e48064-e

21. Smith RE, Zweerink HJ, Joklik WK. Polypeptide components of virions, top component and cores of reovirus type 3. Virology **1969**;39:791-810
22. Fallaux FJ, Kranenburg O, Cramer SJ, Houweling A, Van Ormondt H, Hoeben RC, *et al.* Characterization of 911: a new helper cell line for the titration and propagation of early region 1-deleted adenoviral vectors. Human gene therapy **1996**;7:215-22
23. Hiller BE, Berger AK, Danthi P. Viral gene expression potentiates reovirus-induced necrosis. Virology **2015**;484:386-94
24. Hingorani SR, Wang L, Multani AS, Combs C, Deramaudt TB, Hruban RH, *et al.* Trp53R172H and KrasG12D cooperate to promote chromosomal instability and widely metastatic pancreatic ductal adenocarcinoma in mice. Cancer cell **2005**;7:469-83
25. Benonisson H, Altıntaş I, Sluijter M, Verploegen S, Labrijn AF, Schuurhuis DH, *et al.* CD3-Bispecific Antibody Therapy Turns Solid Tumors into Inflammatory Sites but Does Not Install Protective Memory. Molecular cancer therapeutics **2019**;18:312-22
26. Rozanov DV, Rozanov ND, Chiotti KE, Reddy A, Wilmarth PA, David LL, *et al.* MHC class I loaded ligands from breast cancer cell lines: A potential HLA-I-typed antigen collection. J Proteomics **2018**;176:13-23
27. Mijatovic-Rustempasic S, Tam KI, Kerin TK, Lewis JM, Gautam R, Quaye O, *et al.* Sensitive and specific quantitative detection of rotavirus A by one-step real-time reverse transcription-PCR assay without antecedent double-stranded-RNA denaturation. Journal of clinical microbiology **2013**;51:3047-54
28. Brahmer JR, Tykodi SS, Chow LQM, Hwu W-J, Topalian SL, Hwu P, *et al.* Safety and activity of anti-PD-L1 antibody in patients with advanced cancer. The New England journal of medicine **2012**;366:2455-65
29. Royal RE, Levy C, Turner K, Mathur A, Hughes M, Kammula US, *et al.* Phase 2 Trial of Single Agent Ipilimumab (Anti-CTLA-4) for Locally Advanced or Metastatic Pancreatic Adenocarcinoma. Journal of Immunotherapy **2010**;33:828-33
30. Lee JW, Komar CA, Bengsch F, Graham K, Beatty GL. Genetically Engineered Mouse Models of Pancreatic Cancer: The KPC Model (LSL-Kras(G12D/+) ;LSL-Trp53(R172H/+) ;Pdx-1-Cre), Its Variants, and Their Application in Immuno-oncology Drug Discovery. Curr Protoc Pharmacol **2016**;73:14.39.1-14.39.20
31. Prestwich RJ, Ilett EJ, Errington F, Diaz RM, Steele LP, Kottke T, *et al.* Immune-mediated antitumor activity of reovirus is required for therapy and is independent of direct viral oncolysis and replication. Clin Cancer Res **2009**;15:4374-81
32. Fransen MF, Schoonderwoerd M, Knopf P, Camps MG, Hawinkels LJ, Kneilling M, *et al.* Tumor-draining lymph nodes are pivotal in PD-1/PD-L1 checkpoint therapy. JCI Insight **2018**;3:e124507
33. Mosely SIS, Prime JE, Sainson RCA, Koopmann J-O, Wang DYQ, Greenawalt DM, *et al.* Rational Selection of Syngeneic Preclinical Tumor Models for Immunotherapeutic Drug Discovery. Cancer Immunology Research **2017**;5:29-41
34. Iorns E, Drews-Elger K, Ward TM, Dean S, Clarke J, Berry D, *et al.* A new mouse model for the study of human breast cancer metastasis. PLoS One **2012**;7:e47995
35. Twumasi-Boateng K, Pettigrew JL, Kwok YYE, Bell JC, Nelson BH. Oncolytic viruses as engineering platforms for combination immunotherapy. Nature Reviews Cancer **2018**;18:419-32
36. Harrington KJ, Vile RG, Melcher A, Chester J, Pandha HS. Clinical trials with oncolytic reovirus: moving beyond phase I into combinations with standard therapeutics. Cytokine Growth Factor Rev **2010**;21:91-8
37. Baum A, García-Sastre A. Induction of type I interferon by RNA viruses: cellular receptors and their substrates. Amino Acids **2010**;38:1283-99
38. Goubau D, Schlee M, Deddouche S, Pruijssers AJ, Zillinger T, Goldeck M, *et al.* Antiviral immunity via RIG-I-mediated recognition of RNA bearing 5′-diphosphates. Nature **2014**;514:372-5

39. Dai P, Wang W, Yang N, Serna-Tamayo C, Ricca JM, Zamarin D*, et al.* Intratumoral delivery of inactivated modified vaccinia virus Ankara (iMVA) induces systemic antitumor immunity via STING and Batf3-dependent dendritic cells. Science Immunology **2017**;2:eaal1713
40. Ilett EJ, Prestwich RJ, Kottke T, Errington F, Thompson JM, Harrington KJ*, et al.* Dendritic cells and T cells deliver oncolytic reovirus for tumour killing despite pre-existing anti-viral immunity. Gene Ther **2009**;16:689-99
41. Berkeley RA, Steele LP, Mulder AA, van den Wollenberg DJM, Kottke TJ, Thompson J*, et al.* Antibody-Neutralized Reovirus Is Effective in Oncolytic Virotherapy. Cancer Immunology Research **2018**;6:1161-73
42. Adair RA, Roulstone V, Scott KJ, Morgan R, Nuovo GJ, Fuller M*, et al.* Cell Carriage, Delivery, and Selective Replication of an Oncolytic Virus in Tumor in Patients. Science translational medicine **2012**;4:138ra77-ra77
43. Andtbacka RHI, Kaufman HL, Collichio F, Amatruda T, Senzer N, Chesney J*, et al.* Talimogene Laherparepvec Improves Durable Response Rate in Patients With Advanced Melanoma. Journal of Clinical Oncology **2015**;33:2780-8
44. Speck T, Heidbuechel JPW, Veinalde R, Jaeger D, von Kalle C, Ball CR*, et al.* Targeted BiTE Expression by an Oncolytic Vector Augments Therapeutic Efficacy Against Solid Tumors. Clinical Cancer Research **2018**;24:2128-37
45. Fajardo CA, Guedan S, Rojas LA, Moreno R, Arias-Badia M, de Sostoa J*, et al.* Oncolytic Adenoviral Delivery of an EGFR-Targeting T-cell Engager Improves Antitumor Efficacy. Cancer research **2017**;77:2052-63
46. Yu F, Wang X, Guo ZS, Bartlett DL, Gottschalk SM, Song X-T. T-cell engager-armed oncolytic vaccinia virus significantly enhances antitumor therapy. Molecular Therapy **2014**;22:102-11
47. Freedman JD, Hagel J, Scott EM, Psallidas I, Gupta A, Spiers L*, et al.* Oncolytic adenovirus expressing bispecific antibody targets T-cell cytotoxicity in cancer biopsies. EMBO Mol Med **2017**;9:1067-87
48. Yu L, Wang J. T cell-redirecting bispecific antibodies in cancer immunotherapy: recent advances. Journal of Cancer Research and Clinical Oncology **2019**;145:941-56
49. Haense N, Atmaca A, Pauligk C, Steinmetz K, Marmé F, Haag GM*, et al.* A phase I trial of the trifunctional anti Her2 × anti CD3 antibody ertumaxomab in patients with advanced solid tumors. BMC Cancer **2016**;16:420
50. Ishiguro T, Sano Y, Komatsu SI, Kamata-Sakurai M, Kaneko A, Kinoshita Y*, et al.* An anti-glypican 3/CD3 bispecific T cell-redirecting antibody for treatment of solid tumors. Science translational medicine **2017**;9
51. O'Rourke DM, Nasrallah MP, Desai A, Melenhorst JJ, Mansfield K, Morrissette JJD*, et al.* A single dose of peripherally infused EGFRvIII-directed CAR T cells mediates antigen loss and induces adaptive resistance in patients with recurrent glioblastoma. Science translational medicine **2017**;9:eaaa0984
52. Holland CJ, Crean RM, Pentier JM, de Wet B, Lloyd A, Srikannathasan V*, et al.* Specificity of bispecific T cell receptors and antibodies targeting peptide-HLA. The Journal of Clinical Investigation **2020**;130:2673-88

SUPPLEMENTARY METHODS

Cell culture

All cells were cultured at 37 °C in a humidified atmosphere containing 5% CO_2 in Iscove's Modified Dulbecco's medium (IMDM; Invitrogen) supplemented with 8% fetal calf serum (FCS; Bodinco, Alkmaar, The Netherlands), 2mM L-glutamine (Gibco), 100 µg/mL penicillin and 100 µg/mL streptomycin (Gibco). The tumor cell line TC-1 was additionally cultured in the presence of 400 µg/ml Geneticin (G418; Life Technologies), 1% nonessential amino acids (Life Technologies), and 1 mM sodium pyruvate (Life Technologies). Cell lines were assured to be free of *Mycoplasma* by regular PCR analysis. Authentication of the cell lines was done by Short Tandem Repeat (STR) profiling (IDEXX BioAnalytics, Ludwigsburg, Germany) and cells of low passage number were used for all experiments.

In vivo αPD-L1 treatment

Mice were treated on indicated days with intraperitoneal injections of 200 µg PD-L1-blocking antibody (clone 10F.9G2; GoInVivo™ Purified anti-mouse CD274 Antibody; BioLegend).

CsCl purification of reovirus stock

For purification, a freeze-thaw lysate containing reovirus particles was incubated with 0,1% Triton (Sigma-Aldrich, Zwijndrecht, the Netherlands) and 25 units/ml Benzonase (Santa Cruz, Bio-Connect B.V. Huissen, the Netherlands) for 15 min on ice followed by 15 min at 37 °C. After two extractions with Halotec CL10 (FenS B.V. Goes, the Netherlands) to remove cellular debris, the cleared lysate was loaded onto a discontinuous CsCl gradient (1.45 and 1.2 g/cm^3 in phosphate-buffered saline (PBS)). After centrifugation in a SW28 rotor (Beckman Coulter, Woerden, the Netherlands) at 69000 × g for 14 hours at 4 °C, the lower band containing the infectious particles was harvested and desalted in an Amicon Ultra 100K device according to the manufacturer's protocol (Millipore, Merck Chemicals BV, Amsterdam, the Netherlands). The CsCl-purified reoviruses were recovered in reovirus storage buffer (RSB: 10mM Tris-HCl; pH 7.5, 150mM NaCl, 10mM $MgCl_2 \cdot 6$ H2O), aliquoted and stored at 4 °C until use.

In vitro viability assays

The oncolytic capacity of reovirus was assessed using a colorimetric assay to determine metabolic activity. In short, KPC3 and B16.F10 cells were seeded in a concentration of 5000 (KPC3) and 2500 (B16.F10) cells/well and left to attach overnight. The next day, cells were infected with designated MOIs of reovirus. Cell viability was assessed after 48 hours using the CellTiter 96® AQ_{ueous} One Solution Cell Proliferation Assay (Promega). 20 µL/well of CellTiter 96® AQ_{ueous} One Solution Reagent was added for two hours. The ability of CD3xTRP1 bsAbs to induce specific killing was assessed using a colorimetric method for quantifying cellular cytotoxicity. In short, KPC3, KPC3.TRP1 and B16.F10 cells were irradiated at 6000 RAD and plated at a concentration of 30.000 cells/well. Splenocytes were isolated from a naive C57BL/6J mice and B cells were

removed by passaging through nylon wool before use. Splenocytes were added in an E/T ratio of 5:1 and then CD3xTRP1 or CD3xFluorescein bsAbs (CD3xcntrl) were added in a concentration of 1 µg/mL. 48 hours after incubation, 20 µL of Triton-X100 was added to wells containing tumor cells alone to serve as a positive control. 50 µL of supernatant was harvested of all conditions and incubated for 30 minutes with 50 µL of lactate dehydrogenase reaction mix (Pierce LDH Cytotoxicity Assay Kit, ThermoFisher Scientific). Absorbance was measured at 490 using a SpectraMax iD3 multi-mode plate reader (Molecular Devices). Viability was normalized to the viability of non-infected conditions, and % of cytotoxicity was calculated using the positive control as 100 % cytotoxicity. All conditions were performed in triplicate.

Cell preparation and flow cytometry

Tumors were minced in small pieces and additionally incubated with Liberase TL (Roche) for 15 minutes at 37 °C. The reaction was stopped by the addition of medium and the mixture was gently dissociated into a single-cell suspension over a cell strainer. Single-cell suspensions of splenocytes were resuspended in lysis buffer to remove all red blood cells before use. Cells were incubated with Zombie AquaTM Fixable Viability Dye (Biolegend) in PBS at room temperature followed by incubation with 2.4G2 FcR blocking antibodies (clone 2.4G2; BD Biosciences) in FACS buffer (PBS, 0.5% BSA and 1% NaAz) before surface marker staining (**Table S1**). If applicable, cells were fixed and stained for transcription factors and nuclear proteins using the Foxp3 / Transcription Factor Staining Buffer Set (eBiosciences) according to manufacturers' instructions. TRP1 expression on KPC3.TRP1 tumor cells was measured using the αTRP1 primary antibody (clone: TA99) followed by a secondary Alexa Fluor 647-labeled anti-mouse IgG (BioLegend). HER2 expression on BT474 tumor cells was measured using the anti-erbB-2 (Her-2/neu) primary antibody (clone: 4D5-8) followed by a secondary PE-labeled anti-rabbit IgG (BioLegend). The frequency of $\sigma3^+$ cells was determined as a method of quantifying the infection efficiency of reovirus. Cells were harvested 48 hours after infection and fixed with Fixation Buffer (BioLegend) according to the manufacturer's instructions. Afterward, cells were washed with Permeabilization Wash Buffer (BioLegend) and stained with 4F2 hybridoma supernatant (dilution 1:500), recognizing the σ3 protein of reovirus T3D (Developmental Studies Hybridoma Bank) followed by a secondary Alexa Fluor 647-labeled anti-mouse IgG (BioLegend). After completion of staining protocols, samples were fixed in 1% paraformaldehyde and acquired using a BD LSRFortessa™ X20 cell analyzer (BD Biosciences) within 24 hours. Flow cytometry data was analyzed using FlowJo™ Software Version 10 (Becton, Dickinson, and Company).

Ex vivo analysis of TIL specificity

To determine the specificity of T cells in the tumor and spleen, KPC3-bearing mice were treated with the standard regimen reovirus as described above. Single-cell suspensions of individual tumors and spleens, collected at seven days after the last reovirus injection, were co-cultured with irradiated (6000 RAD) target cells. The irrelevant tumor cell line TC-1 was used as a target to facilitate reovirus replication and PMA (20 ng/mL)

and ionomycin (1 µg/mL) were used as positive control. After 1 hour of co-incubation, BD GolgiPlug™ (BD Biosciences) was added in a 1:1000 dilution. After an additional 5 hours, cells were washed and stained for surface markers. Afterward, cells were fixed, permeabilized, and stained for intracellular markers using the Foxp3/Transcription Factor Staining Buffer Set (eBiosciences) according to manufacturers' instructions. After completion of the staining protocol, samples were fixed, measured, and analyzed as described above.

RNA isolation

From *in vitro* samples, total RNA was isolated from cell pellets using the NucleoSpin® RNA Kit (Macherey-Nagel™) according to the manufacturer's instructions. For *in vivo* samples, a representative snap-frozen proportion (10-30 mg) of each tumor or organ was disrupted using a stain-less bead and the TissueLyser LT (Qiagen). Total RNA of *in vivo* samples was using the ReliaPrep™ RNA Tissue Miniprep System (Promega) according to manufacturer's protocol. RNA quality and integrity were determined using the Experion™ Automated Electrophoresis System (Bio-Rad).

RT-qPCR analysis

For S4 analysis, 150 ng of RNA was used to generate cDNA with primer S4EndR (GATGAATGAAGCCTGTCCCACGTCA) and GoScript™ Reverse Transcriptase (Promega). For assessing the transcription levels of host genes *Ifit-1, Ifit-3, Oas1b, Ddx58, Cxcl10, Ccl5,* and *β2M*, 500 ng of RNA was used to generate cDNA using the High-Capacity RNA-to-cDNA™ Kit (ThermoFisher Scientific) according to the manufacturer's protocol. Subsequent qPCR analysis was performed using the Bio-Rad iQ™ SYBR® Green Supermix (Bio-Rad) and the primer sets are displayed in (**Table S2**). The expression of host genes was normalized to reference genes *Mzt2, Ptp4a2, and Ubc* using the Bio-Rad CFX Manager 3.1 Software (Bio-Rad). All primers were quality controlled by assessing the slope, efficiency, and R^2 value of dilution series using cDNA that was synthesized from murine reference RNA. All samples were measured in technical duplicates or triplicates. The used PCR program consisted of the following steps: (1) 3 min at 95 °C; (2) 40 cycles of 10 s at 96 °C followed by 30 s at 60 °C and plate read; (3) 10 s at 95 °C; (4) Melt curve 65–95 °C with an increment of 0.2 °C every 10 s, and plate read.

Immunohistochemistry

Formaldehyde-fixed, paraffin-embedded tissue sections were stained for reoviral protein σ3 or murine CD3. Formalin-fixed tumor pieces were embedded in paraffin and then sectioned randomly at 5 µm and placed on Superfrost® Plus slides (VWR). Sections were dried overnight at 37 °C and stored at 4 °C until staining. Slides were deparaffinized and endogenous peroxidase was blocked with 0,3% hydrogen peroxidase (VWR) in methanol for 20 minutes. After rehydration, antigen retrieval was performed by boiling slides for 10 minutes in 0,01M sodium citrate (Merck). Non-specific binding was blocked using SuperBlock™ (ThermoFisher Scientific) before overnight incubation at 4 °C with rabbit anti-mouse CD3ε D7A6E™ XP® mAb (1:200; Cell Signaling Technology), rat

anti-mouse CD8a (clone 4SM15, 1:1600; eBioscience™) or 4F2 hybridoma supernatant which recognizes the σ3 protein of reovirus (1:150; Developmental Studies Hybridoma Bank). Hereafter, samples were incubated for 30 min at RT with biotinylated goat anti-rabbit, rabbit anti-rat, or goat anti-mouse secondary antibodies (1:200; Agilent), followed by incubation with avidin-biotin complex (VECTASTAIN® Elite® ABC HRP Kit; Vector Laboratories). Peroxidase activity was detected using the 2-component liquid DAB+ system (Agilent) according to the manufacturer's instructions for 5 min. Slides were counterstained in hematoxylin (Sigma Aldrich), dehydrated, and mounted using Entellan (Sigma Aldrich). Control sections were processed in parallel, but without incubation with primary antibody. No labeling was observed in the control sections.

SUPPLEMENTARY FIGURES

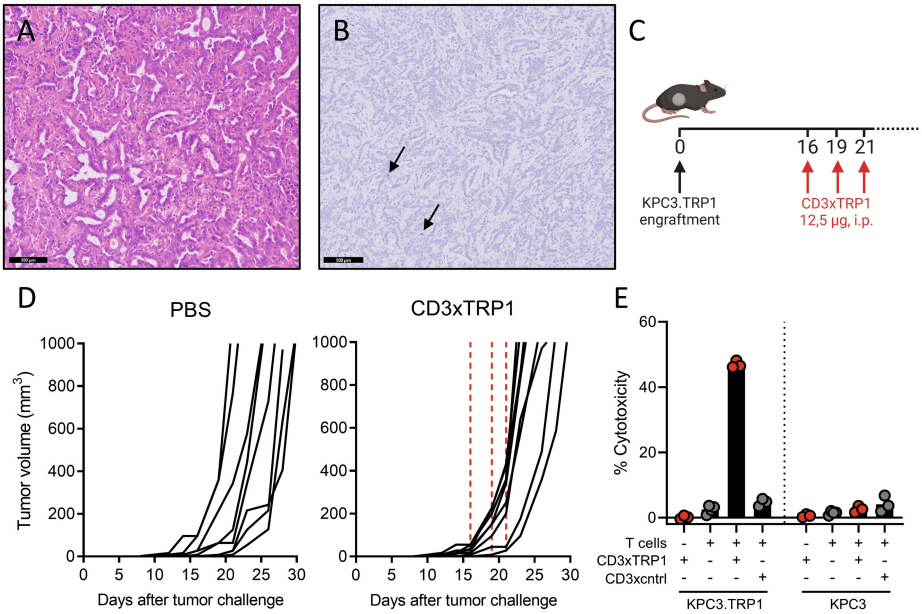

Figure S1. CD3xTRP1 bsAb treatment is not effective in a therapeutic setting in the KPC3.TRP1 model. Hematoxylin and eosin (H&E) staining (**A**) or CD3 immunohistochemical staining (**B**) of representative untreated KPC3 tumor at a size of 1000 mm^3. Arrows indicate $CD3^+$ cells. Scale bar equals 100 µm. (**C**) *In vivo* treatment schedule. Mice (n=8/group) with established KPC3.TRP1 tumors were treated i.p. with 12.5 µg CD3xTRP1 on indicated days, after which tumor growth was monitored. (**D**) Individual tumor growth curves of mice treated with PBS or CD3xTRP1 BsAb. Dashed red vertical lines indicate timing of injection with CD3xTRP1. (**E**) Percentages of cytotoxicity of KPC3.TRP1 or KPC3 cells after *in vitro* co-culture with naive T cells and CD3xTRP1 or CD3xcntrl bsAbs (CD3xFluorescein; bAb0161, Absolute Antibody). Data represent mean±SEM of triplicates. BsAb, bispecific antibody.

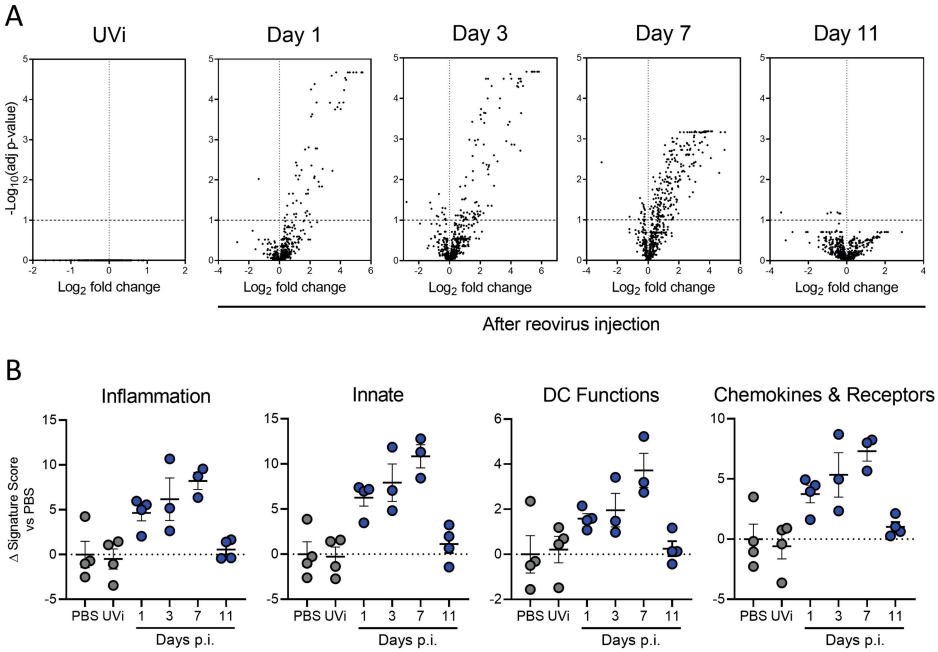

Figure S2. Transcriptomic changes after treatment with replication-competent reovirus. (**A**) Volcano plots showing the differentially expressed genes analyzed by NanoString at various timepoints after treatment with replication-competent reovirus or day 3 after treatment with UVi, normalized versus PBS (n=3-4/group). Horizontal dashed line indicates FDR p-value of 0.1. (**B**) Changes in signature scores on indicated days after reovirus treatment. All scores are normalized for average score of PBS. Data are presented as mean±SEM. UVi, UV-inactivated reovirus.

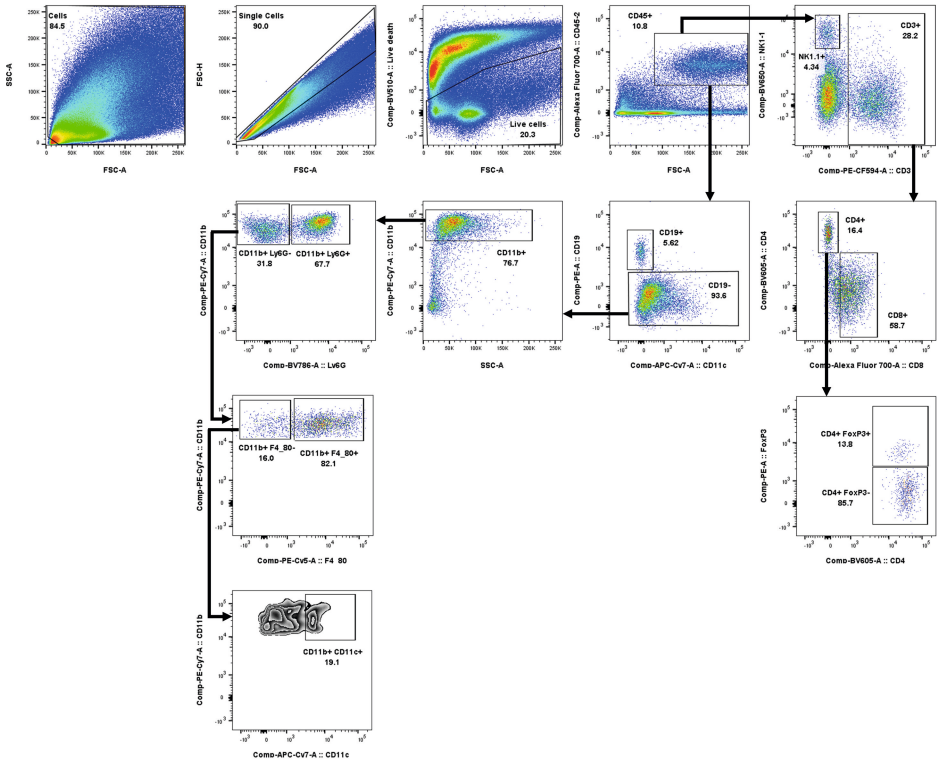

Figure S3. Gating strategy for flow cytometric analyses of the lymphoid and myeloid cell compartment in the tumor after reovirus treatment. Cells of the lymphoid and myeloid compartment were gated according to visualized strategy. Specific antibodies used for flow cytometry can be found in **Table S1**. Data was analyzed by FlowJo™ software.

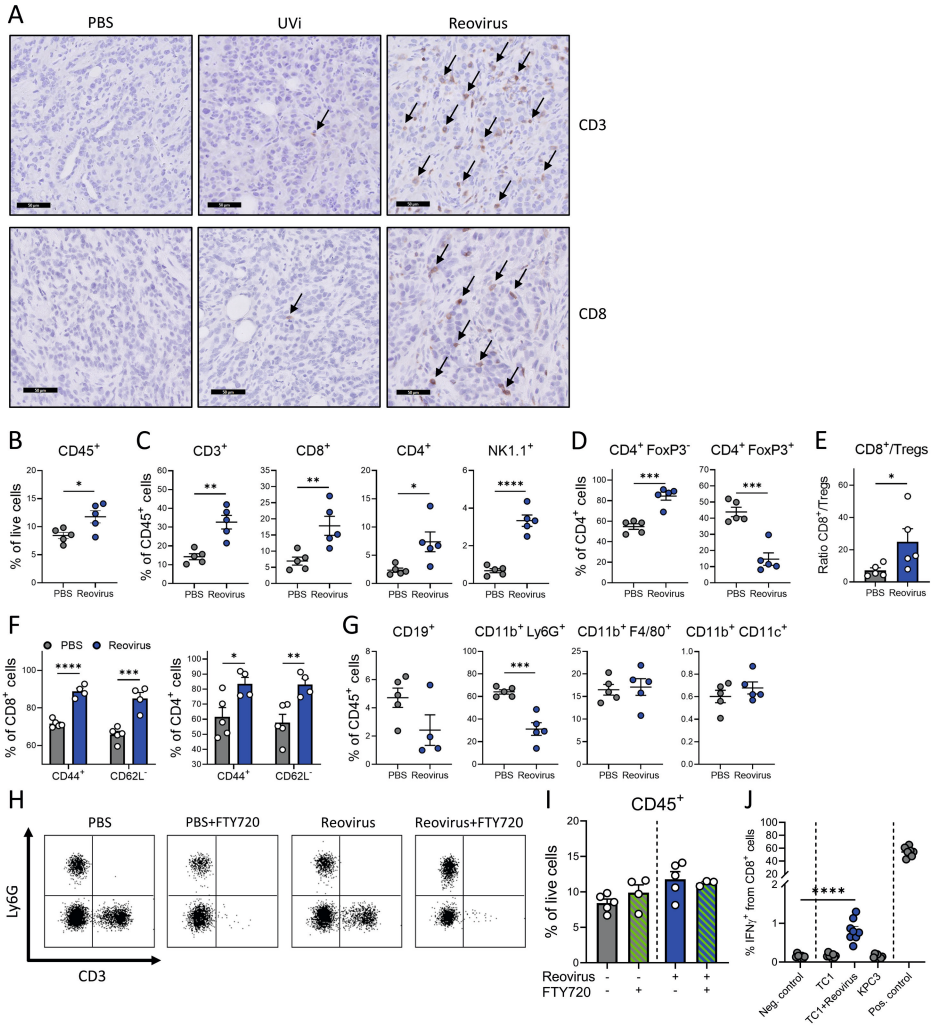

Figure S4. Extended analysis of changes in immune cell composition in the tumor 5 days after reovirus treatment. (**A**) CD3 and CD8 immunohistochemical staining of representative KPC3 tumors injected with PBS, UVi or replication-competent reovirus. Arrows indicate CD3$^+$ or CD8$^+$ cells. Scale bar equals 50 µm. (**B**) Frequency of CD45$^+$ immune cells out of all live cells. (**C**) Frequency of CD3$^+$, CD8$^+$ and CD4$^+$ T cells and NK1.1$^+$ cells out of CD45$^+$ immune cells in tumors after administration of reovirus or PBS. (**D**) Frequency of CD4$^+$ FoxP3$^-$ (conventional CD4$^+$ T cells) and CD4$^+$ FoxP3$^+$ (regulatory T cells). (**E**) Ratio between CD8$^+$ T cells and CD4$^+$FoxP3$^+$ cells (regulatory T cells) within the CD45$^+$ immune cell population in the tumor after treatment with reovirus or PBS. Statistical difference between groups is determined using a Mann Whitney U test. (**F**) Activation status of intratumoral CD8$^+$ and CD4$^+$ T cells after reovirus or PBS treatment. (**G**) Percentages of other immune cells within the CD45$^+$ population after treatment with reovirus or PBS. Significance of data visualized in B-D, F and G is determined using unpaired t tests. (**H**) Presence of CD3$^+$ T cells and Ly6G$^+$ cells in tail blood of mice treated as indicated, without or with FTY720. Representative flow cytometry dot plot of one mouse per group is shown. (**I**) Frequency of CD45$^+$ immune cells in de tumor. Data is representative for 2 independent experiments. (**J**) Presence of IFNγ$^+$ CD8$^+$ cells in the spleen after ex vivo co-culture with indicated targets. All data are presented as mean±SEM (n=5/group for A-I, n=8/group for J). In figure I, significance between groups is determined using an ordinary one-way ANOVA with Tukey's post-hoc test. In (J), significance versus negative control is determined using an unpaired t test. Significance levels are indicated with asterisks, with *p<0.05, **p<0.01, ***p<0.001, and ****p<0.0001. UVi, UV-inactivated reovirus.

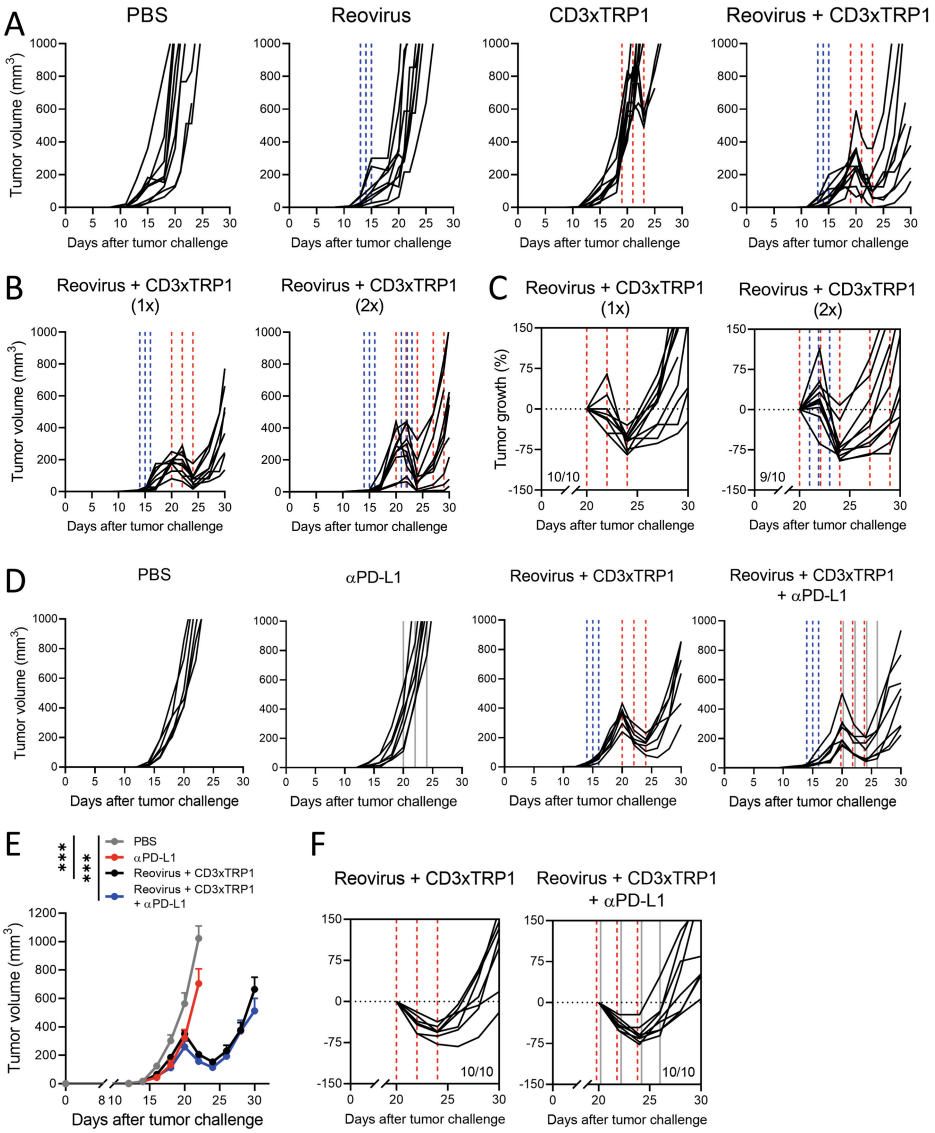

Figure S5. Strategies to prevent immune escape after combined reovirus and CD3xTRP1 bsAb combination treatment. (**A**) Individual tumor growth curves of experiment described in Figure 4B. Dashed vertical lines indicate timing of treatment with Reovirus (blue) or CD3xTRP1 (red). (**B**) Individual tumor growth curves of groups receiving one round or two rounds of reovirus + CD3xTRP1 therapy (n=10/group). (**C**) Relative changes in tumor volume of individual mice from the start of CD3xTRP1 bsAb treatment. Indicated is the number of mice with tumor regressions. (**D**) Individual growth curves of KPC3.TRP1-bearing mice receiving indicated treatments. Grey lines indicate timing of treatment with αPD-L1. (**E**) Average tumor growth curves. Differences in mean tumor volumes versus PBS treatment on day 22 is determined by ordinary one-way ANOVA with Dunnett's post-hoc test. (**F**) Relative changes in tumor volume from start of CD3xTRP1 bsAb treatment. Indicated is the number of mice with tumor regressions. All data are presented as mean±SEM. Significance level: ***p<0.001. BsAb, bispecific antibody.

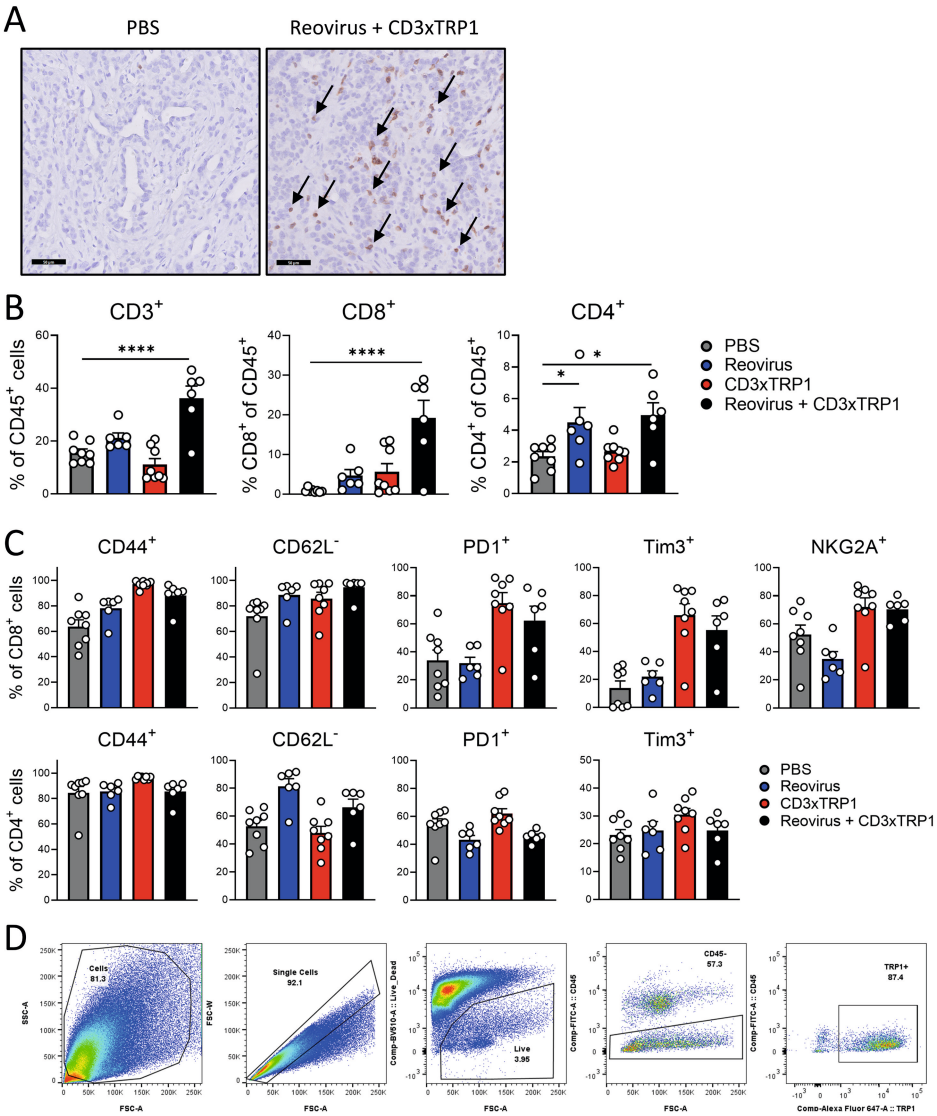

Figure S6. Analysis of mechanisms underlying escape to reovirus and CD3xTRP1 bsAb combination treatment. (**A**) Representative images obtained from immunohistochemical CD3 staining (light brown) of tumors treated with PBS or reovirus + CD3xTRP1. Arrows indicate $CD3^+$ cells. Scale bars equal 100 µm. (**B**) Flow cytometric analysis of the frequency of tumor-infiltrating T cells (TILs) in end stage tumor samples (n=6-8/group). Significance versus PBS treatment is determined using an ordinary one-way ANOVA with Dunnett's post-hoc test. (**C**) Expression of activation markers and checkpoint receptors on TILs. All data are presented as mean±SEM with white dots indicating individual mice. (**D**) Gating strategy to determine TRP1 expression by a 2-step flow cytometry protocol. A sample from the PBS group is depicted. Significance levels are indicated with asterisks, with *p<0.05, **p<0.01, ***p<0.001, and ****p<0.0001. BsAb, bispecific antibody.

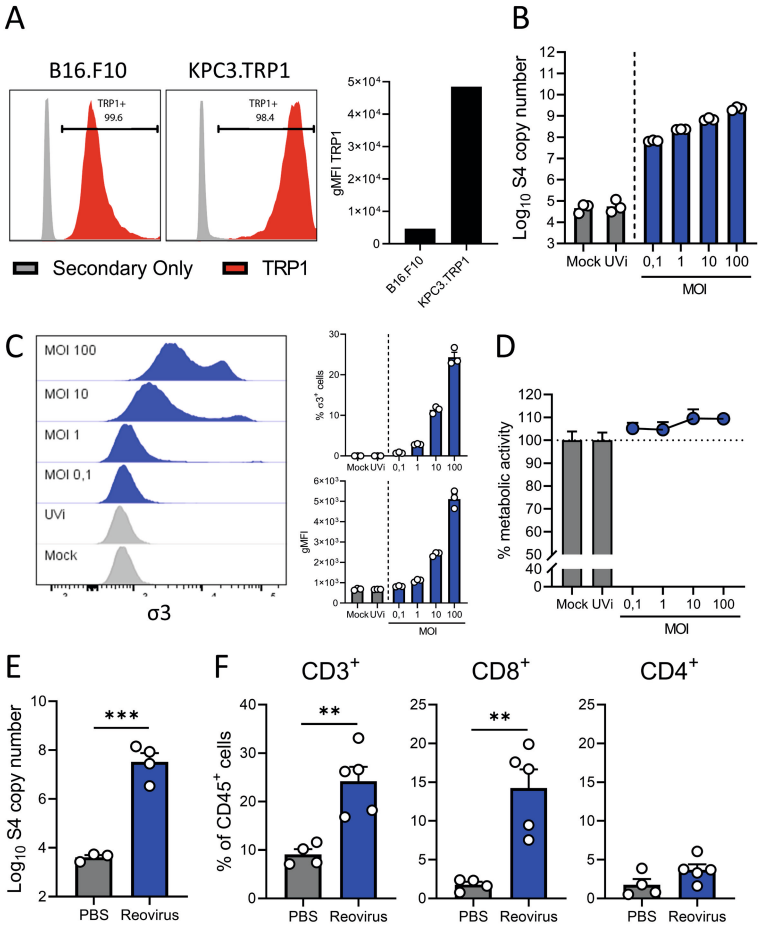

Figure S7. Characterization of reovirus efficacy in B16.F10. (**A**) TRP1 expression percentages and intensities on B16.F10 and KPC3.TRP1 cells, as analysed by flow cytometry using a 2-step protocol. (**B**) Number of reovirus S4 copies in B16.F10 cells after reovirus infection. B16.F10 cells (62.500/well) were infected with increasing MOIs of reovirus, or PBS (Mock) or UVi (equal number of viral particles as MOI 100) as controls. Samples (n=3) were harvested 24 hours after infection and the number of viral S4 copies was determined by RT-qPCR. (**C**) Frequency of $\sigma3^+$ B16.F10 cells 48 hours after infection with increasing MOIs of reovirus (blue histograms), or PBS or UVi as controls (grey histograms). (**D**) Analysis of oncolytic activity of reovirus. B16.F10 cells (2500/well) were plated and infected with reovirus or controls. Metabolic activity was determined 48 hours after infection. (**E**) S4 copy numbers in tumors harvested 5 days after reovirus treatment (n=3-4/group). (**F**) Flow cytometric analysis of the frequency of tumor-infiltrated T cells (TILs) in B16.F10 tumor samples, 7 days after reovirus treatment (n=3-4/group). All data are presented as mean±SEM and individual values. In figures E-F, significance versus PBS treatment is determined using an unpaired t test. Significance levels are indicated with asterisks, with *p<0.05, **p<0.01, and ***p<0.001. UVi, UV-inactivated reovirus. MOI, multiplicity of infection.

SUPPLEMENTARY TABLES

Table S1. List of antibodies used for flow cytometric analysis.

	Marker	*Clone*	*Fluorochrome*	*Supplier*
Lymphoid panel	CD45.2	104	APC-Cy7	eBioscience
	CD3	145-2C11	PE-CF594	BD Biosciences
	CD8α	53-6.7	Alexa Fluor 700	eBioscience
	CD4	RM4-5	BV605	BioLegend
	CD44	IM-7	BV785	BioLegend
	CD62L	MEL-14	BV421	BioLegend
	NK1.1	Pk136	BV650	BD Biosciences
	PD-1	RMP1-30	FITC	eBioscience
	Tim3	RMT3-23	APC	BioLegend
	NKG2A	16A11	PE	eBioscience
	CD43	1b11	PE-Cy5	BioLegend
	KLRG-1	2F1	PE-Cy7	eBioscience
Myeloid panel	CD45.2	104	FITC	BioLegend
	CD19	eBio1D3	PE	eBioscience
	CD11b	M1/70	PE-Cy7	BioLegend
	Ly6G	1A8	BV785	BioLegend
	F4/80	BM8	PE-Cy5	BioLegend
	CD11c	N418	APC-Cy7	BioLegend
Treg panel	CD45.2	104	FITC	BioLegend
	CD3	145-2C11	PE-CF594	BD Biosciences
	CD8α	53-6.7	Alexa Fluor 700	eBioscience
	CD4	RM4-5	BV605	BioLegend
	FoxP3	FJK-16s	PE	eBioscience
	Ki67	B56	BV711	BD Biosciences
Intracellular T-cell activation panel	CD45.2	104	APC-Cy7	eBioscience
	CD3	145-2C11	PE-CF594	BD Biosciences
	CD8α	53-6.7	Alexa Fluor 700	eBioscience
	INFγ	XMG1.2	APC	BioLegend

Table S2. List of primers used for RT-qPCR analysis.

Gene	*Forward*	*Reverse*
S4Q	5′-CGCTTTTGAAGGTCGTGTATCA-3′	5′-CTGGCTGTGCTGAGATTGTTTT-3′
Ifit-1	5′-CTGGACAAGGTGGAGAAGGT-3′	5′-AGGGTTTTCTGGCTCCACTT-3′
Ifit-3	5′-GTGCAACCAGGTCGAACATT-3′	5′- AGGTGACCAGTCGACGAATT-3′
Oas1b	5′-AGCATGAGAGACGTTGTGGA-3′	5′-GCGTAGAATTGTTGGTTAGGCT-3′
Ddx58	5′-AAGGCCACAGTTGATCCAAA-3′	5′-TTGGCCAGTTTTCCTTGTCG-3′
Cxcl10	5′-ACGAACTTAACCACCATCT-3′	5′-TAAACTTTAACTACCCATTGATACATA-3′
Ccl5	5′-ATTGCTTGCTCTAGTCCTA-3′	5′-ATGCTGATTTCTTGGGTTT-3′
β2M	5′-CTCGGTGACCCTGGTCTTT-3′	5′-CCGTTCTTCAGCATTTGGAT-3′
Mzt2	5′-TCGGTGCCCATATCTCTGTC-3′	5′-CTGCTTCGGGAGTTGCTTTT-3′
Ptp4a2	5′-AGCCCCTGTGGAGATCTCTT-3′	5′-AGCATCACAAACTCGAACCA-3′
Ubc	5′-GCCCAGTGTTACCACCAAGA-3′	5′-CCCATCACACCCAAGAACA-3′